The American Journal of Pathology, Vol. 171, No. 3, September 2007

DOI: 10.2353/ajpath.2007.070345

Neurobiology

Early Axonopathy Preceding Neurofibrillary Tangles in Mutant Tau Transgenic Mice

Karelle Leroy,* Alexis Bretteville,† Katharina Schindowski,† Emmanuel Gilissen,* Michèle Authelet,* Robert De Decker,* Zehra Yilmaz,* Luc Buée,† and Jean-Pierre Brion*

From the Laboratory of Histology, Neuroanatomy, and Neuropathology, School of Medicine, Université Libre de Bruxelles, Brussels, Belgium; and Inserm U837 and Institut de Médecine Prédictive et Recherche Thérapeutique,† Jean-Pierre Aubert Research Centre, Faculté de Médecine, Lille, France*

Neurodegenerative diseases characterized by brain and spinal cord involvement often show widespread accumulations of tau aggregates. We have generated a transgenic mouse line (Tg30tau) expressing in the forebrain and the spinal cord a human tau protein bearing two pathogenic mutations (P301S and G272V). These mice developed age-dependent brain and hippocampal atrophy, central and peripheral axonopathy, progressive motor impairment with neurogenic muscle atrophy, and neurofibrillary tangles and had decreased survival. Axonal spheroids and axonal atrophy developed early before neurofibrillary tangles. Neurofibrillary inclusions developed in neurons at 3 months and were of two types, suggestive of a selective vulnerability of neurons to form different types of fibrillary aggregates. A first type of tau-positive neurofibrillary tangles, more abundant in the forebrain, were composed of ribbon-like 19-nm-wide filaments and twisted paired helical filaments. A second type of tau and neurofilament-positive neurofibrillary tangles, more abundant in the spinal cord and the brainstem, were composed of 10-nm-wide neurofilaments and straight 19-nm filaments. Unbiased stereological analysis indicated that total number of pyramidal neurons and density of neurons in the lumbar spinal cord were not reduced up to 12 months in Tg30tau mice. This Tg30tau model thus provides evidence that axonopathy precedes tangle formation and that both lesions can be dissociated from overt neuronal loss in selected brain areas but not from neuronal dysfunction. ***(Am J Pathol 2007, 171:976–992; DOI: 10.2353/ajpath.2007.070345)***

Many neurodegenerative diseases are characterized by the presence of filamentous aggregates in neurons and/or in glial cells and composed of abnormally and hyperphosphorylated forms of the microtubule-associated protein tau. These diseases have been referred to as tauopathies[1] and include some forms of frontotemporal dementia, Pick's disease, progressive supranuclear palsy, corticobasal degeneration, and Alzheimer's disease (AD). Several of these tauopathies are characterized by both cognitive and motor dysfunction and widespread tau pathology in brain, brainstem, and spinal cord. For example, cognitive dysfunction and extrapyramidal symptoms are observed in patients with corticobasal degeneration or progressive supranuclear palsy. In the Guam amyotrophic lateral sclerosis-parkinsonism-dementia complex,[2] and in a subset of frontotemporal dementia,[3] patients present with motorneuron disease and dementia. Although most cases of familial frontotemporal dementia have been recently found to be caused by mutations in the progranulin gene, pathogenic mutations in the tau gene have also been identified in familial forms of frontotemporal lobar degeneration.[4] Tau protein binds to microtubules and is involved in regulation of the stability of microtubules, axoplasmic transport, and axonal differentiation.[5,6] In frontotemporal lobar degeneration with tau gene mutation, their functional effects might be attributable to a loss of function mechanism by virtue of decreased microtubule binding but might also be attributable to a gain of toxic function because some of these

Supported by grants from the Belgian Pôle d'attraction interuniversitaire P6/43, the Fonds pour la Recherche Scientifique Médicale, the Fondation pour la Recherche sur la Maladie d'Alzheimer, the Van Buuren and Génicot Foundations (to J.P.B.), the Centre National de la Recherche Scientifique (to L.B.), the Fédération pour la Recherche sur le Cerveau (to L.B.), Gis-Longévité (to L.B.), the French National Research agency grant ANR-05-BLANC-0320-01 (to L.B.), the Marie Curie Fellowship (to K.S.), and the Région Nord/Pas-de-Calais and Centre Hospitalier Régional Universitaire-Lille (scholarship to A.B.).

Accepted for publication June 7, 2007.

Supplemental material for this article can be found on *http://ajp.amjpathol.org*.

Address reprint requests to Dr. Jean-Pierre Brion, Laboratory of Histology and Neuropathology, Université Libre de Bruxelles, School of Medicine, 808, Route de Lennik, Bldg. G, 1070 Brussels, Belgium. E-mail: jpbrion@ulb.ac.be.

mutations either increase binding to microtubules or increase the aggregation properties of the mutant tau proteins. Transgenic mice overexpressing wild-type human tau[7–12] or pathogenic mutant tau G272V,[13] P301L,[14–16] P301S,[17,18] V337M,[19] and R406W[20,21] have been developed. Neurofibrillary tangles (NFTs) developed in mice expressing mutant tau, but the exact relationship between their formation and neuronal dysfunction and death has not been firmly established. Recent findings suggested that formation of NFTs could be dissociated from other pathologies in P301L mutant tau mice.[16,22] To investigate the relationship between NFT formation and pathological phenotypes in other mutant tau models, we have generated a new transgenic mouse line (Tg30tau) expressing in the forebrain and the spinal cord a human tau protein bearing two pathogenic mutations (P301S and G272V). The P301S tau mutation causes frontotemporal dementia (FTD) or corticobasal degeneration[23] and is associated to widespread tau pathology and an early age of onset. The G272V mutation[24] was identified in a Dutch family with FTDP-17.[25] We previously characterized another tau transgenic line expressing this mutant tau protein only in the forebrain and developing neurofibrillary lesions in the hippocampus and the cortex: these mice showed delayed learning and reduced spatial memory but no motor deficits.[26] The transgenic mice described here developed brain atrophy and a motor neuron disease with axonopathy preceding neurofibrillary pathology and without overt neuronal loss in the hippocampus and the spinal cord, suggesting that these lesions can lead to neuronal dysfunction without cell death in these brain areas.

Materials and Methods

Generation of Transgenic Mice

The generation of transgenic line Tg30tau has been previously reported,[26] but the pathological analysis of line Tg30tau has not been described before and is presented here. These mice express a mutant tau transgene (1N4R human tau isoform) mutated at positions G272V and P301S, under the control of a modified thy-1 promoter to drive expression in neurons.[27,28] Only heterozygous animals were used in the present study; nontransgenic littermates were used as wild-type controls. Transgenic animals were identified by polymerase chain reaction amplification of the tau transgene in genomic DNA as reported.[29] All studies on animals were performed in compliance and following approval of the school of medicine ethics committee for animal care and use.

Motor Testing

Motor deficits in Tg30tau mice were assessed by testing on a Rotarod apparatus (Ugo Basile, Comerio, Italy) at 8, 10, and 12 months of age. Animals were first submitted to training sessions (three trials per day during 3 consecutive days) during which they were placed on the rod rotating at constant speed (4 rpm). Animals were individually separated the day before the test and randomly evaluated on two consecutive test sessions, using an experimental setting of progressive acceleration from 4 to 40 rpm throughout 300 seconds. The latency to fall off the Rotarod was recorded. Animals staying up to 300 seconds were removed from the Rotarod, and their latency to fall recorded as 300 seconds.

Histological Staining

The brains and spinal cords of wild-type and Tg30tau transgenic mice were dissected at 1, 3, 6, and 12 months. After wet weight estimation, tissues were fixed in 10% formalin or in 4% (w/v) paraformaldehyde and embedded in paraffin. Formalin-fixed sections (10-μm thick) were stained with hematoxylin and eosin, with the Nissl method, with the Gallyas silver-staining method, or with Congo Red and thioflavin. Tissue sections were examined with a Zeiss Axioplan microscope (Carl Zeiss GmbH, Jena, Germany) and digital images acquired using an Axiocam HRc camera (Carl Zeiss). The density of Gallyas-positive cell profiles in the cortex, in the hippocampus, and in the spinal cord was expressed as the total number of Gallyas-positive cell profiles visible on whole sagittal (cortex and hippocampus) or coronal (lumbar spinal cord) tissue section of 3-, 6-, and 12-month-old mice ($n = 3$ different animals at each age).

Antibodies

The B19 antibody is a rabbit polyclonal antibody raised to adult bovine tau proteins, reacting with all adult and fetal tau isoforms in bovine, rat, mouse, and human nervous tissue in a phosphorylation-independent manner.[30] The TP20 and M19G rabbit polyclonal antibodies were raised against a synthetic peptide of human tau and react with human tau and not with mouse tau.[8,31] The TP007 and TP70 rabbit polyclonal antibodies were raised against synthetic peptides mapping at the extreme N and C termini of human tau, respectively.[32,33] The anti-cleaved tau (Asp421) mouse monoclonal antibody was purchased from Upstate Biotechnology (Lake Placid, NY). The mouse monoclonal antibody AD2 is specific for tau phosphorylated at Ser396.[31] The AT8, AT180, AT270, and AT100 mouse monoclonal antibodies (purchased from Innogenetics, Ghent, Belgium) are specific for tau phosphorylated at Ser202 and Thr205 (AT8),[34] at Thr231 (AT180), at Thr181 (AT270),[35] and a specific PHF-tau epitope involving phosphorylation at Thr212 and Ser214 (AT100).[36] The mouse monoclonal antibodies PHF-1 (kindly provided by Drs. P. Davies and S. Greenberg, Albert Einstein College of Medicine, Bronx, NY) and AP422 (kindly provided by Drs. M. Hasegawa and M. Goedert, Medical Research Council-Laboratory of Molecular Biology, Cambridge, UK) are specific for tau phosphorylated at Ser396/404 and Ser422, respectively.[37,38] The tau monoclonal antibody MC1 (kindly provided by Dr. P. Davies) recognizes a conformational epitope requiring both an N-terminal fragment and a C-terminal frag-

ment.[39] BioSource (Nivelles, Belgium) provided the phosphospecific rabbit polyclonal tau antibodies to pThr212, pSer214, pSer262, pThr403, and pSer409. The mouse monoclonal antibody to ubiquitin (clone MAB1510) was from Chemicon (Temecula, CA). The mouse monoclonal antibodies to α-tubulin (clone DM1-A), to β-actin (clone AC15), and to GFAP (clone GA5) were from Sigma (Bornem, Belgium). The polyclonal rabbit antibodies to neurofilament L (NA1214) and M (NA1216), to phosphorylated neurofilament H (NA 1211) and the mouse monoclonal antibody to neurofilament H (clone SMI32) and phosphorylated neurofilament H (SMI31) were from Affiniti (Exeter, UK). The anti-phosphotyrosine antibodies 4G10 and PT-66 were purchased from Upstate Biotechnology and Sigma. For detection of Aβ, we used a polyclonal antibody raised to amino acids 12 to 28 of the Aβ peptide.[40]

Several antibodies to protein kinases or phosphatases were also used. The mouse monoclonal antibodies to cdc2 (clone 17) and cdk5 (clone DC17) and polyclonal antibodies to cdk5 (C-8 and H291), p35, ERK1 (C-16), and casein kinase Id (R-19) were purchased from Santa Cruz Biotechnology (Santa Cruz, CA). The mouse monoclonal antibody to ERK1 was from Affiniti and to Jun kinase (phospho Thr183/Tyr185) from Cell Signaling (Suffolk, UK). The anti-GSK-3β (TPK1) antibody was from Transduction Laboratories (San Jose, CA). The antibodies to GSK-3 phosphorylated on Tyr216 were from BioSource and from Upstate Biotechnology. The antibody to active caspase3 was from Promega (Madison, WI).

Preparation of Brain Homogenates and Western Blot Analysis

Brain and spinal cord of Tg30tau and wild-type mice were quickly dissected after lethal anesthesia and separately homogenized in a buffer containing proteases and phosphatase inhibitors (50 mmol/L Tris, 10 mmol/L ethylenediamine tetraacetic acid, pH 7.4, 1 mmol/L phenylmethyl sulfonyl fluoride, 25 μg/ml leupeptin, 25 μg/ml pepstatin, 1 mmol/L Na_3VO_4, 10 mmol/L $Na_4P_2O_7$.10 H_2O, and 20 mmol/L NaF). Samples were mixed with sodium dodecyl sulfate sample buffer containing a reducing agent and then boiled at 100°C for 10 minutes (all done as recommended by Invitrogen). For Western blot analysis, 10 μg of total protein was separated by 10% sodium dodecyl sulfate-polyacrylamide gel electrophoresis (NuPAGE; Invitrogen, Carlsbad, CA), blotted onto nitrocellulose or polyvinylidene difluoride membranes (Hybond and Hybond Phosphate from Amersham/GE Health Care, Orsay, France). The membranes were blocked and incubated with the appropriate primary antibody and then incubated with a horseradish peroxidase-conjugated secondary antibody (goat anti-rabbit A4914 from Sigma-Aldrich, Lyon, France; and horse anti-mouse from Vector Laboratories, Burlingame, CA). Finally, the peroxidase activity was detected with the ECL detection kit and visualized with Hyperfilm ECL (Amersham/GE Health Care).

Immunocytochemistry and Terminal dUTP Nick-End Labeling (TUNEL) Staining

The immunohistochemical labeling was performed using the ABC method. In brief, tissue sections were treated with H_2O_2 to inhibit endogenous peroxidase and incubated with the blocking solution [10% (v/v) normal horse serum in Tris-buffered saline (0.01 mol/L Tris and 0.15 mol/L NaCl, pH 7.4)]. After an overnight incubation with the diluted primary antibody, the sections were sequentially incubated with horse anti-mouse antibodies conjugated to biotin (Vector Laboratories, Burlingame, CA) followed by the ABC complex (Vector). The peroxidase activity was revealed using diaminobenzidine as chromogen. For immunolabeling with the Aβ antibodies, rehydrated tissue sections were pretreated with 100% formic acid for 10 minutes before incubation with the blocking solution.

Double immunolabeling was performed using fluorescent markers. The first antibody was detected using an anti-rabbit or an anti-mouse antibody conjugated to fluorescein isothiocyanate (Jackson, Boston, MA), and the second antibody was detected using an anti-rabbit or an anti-mouse antibody conjugated to biotin, followed by streptavidin conjugated to Alexa 594 (Molecular Probes, Carlsbad, CA). Double immunolabeling was followed by nuclear 4,6-diamidino-2-phenylindole staining. Selected areas in tissue sections were photographed after double-fluorescent immunolabeling and stained with the Gallyas silver staining method to identify neurons containing fibrillary material. The number of phosphotau-positive cell profiles in the cortex, in the hippocampus, and in the gray matter of the spinal cord was determined in 3-, 6-, and 12-month-old mice as described above for Gallyas staining. TUNEL staining was performed on tissue sections to detect DNA cleavage associated with apoptotic cell death using digoxigenin-dUTP, as previously reported.[41]

Stereological Analysis

For stereological analysis, wild-type and transgenic animals were intracardially perfused with 10% (v/v) formalin, and their brain and spinal cord were dissected and embedded in paraffin. Brains and lumbar spinal cord were serially cut in coronal sections (15-μm thickness) that were then stained with Cresyl violet. The total numbers of hippocampal pyramidal cells was estimated in the left hemispheres of 12-month-old transgenic mice (n = 3) and wild-type mice (n = 3). For each animal, 10 coronal sections at 75-μm intervals throughout the hippocampal pyramidal cell layer were used. The pyramidal cell layer was delineated as depicted in Figure 3C. Counting of total numbers of neurons was performed with a $\times$100/1.30 oil objective by using a random-sampling stereological counting tool, the optical fractionator,[42,43] which is implemented within a stereology workstation consisting of a modified light microscope (Leica DMR, Wetzlar, Germany), Leica PL Fluotar objectives ($\times$10/0.30; $\times$100/1.30 oil), a motorized specimen stage for automatic sampling (BioPoint 2; Ludl Elec-

tronic Products, Hawthorne, NY), an electronic microcator (Heidenhain, Traunreut, Germany), a charge-coupled device color video camera (HV-C20A; Hitachi, Tokyo, Japan), and a personnel computer with stereology software (Stereoinvestigator version 5.05.4; MicroBrightField, Inc., Colchester, VT). Optical disectors were automatically randomly distributed throughout the delineated area, and each pyramidal cell whose nuclear top came into focus within an optical disector was counted. Estimated total numbers of pyramidal cells per specimen were hence calculated from the number of counted neurons, the volume of the pyramidal cell layer, and the sampling probability.[44] Supplemental Table 1 (see *http://ajp.amjpathol.org*) summarizes the details of the counting procedure. For measuring the volume of the hippocampal pyramidal cell layer, the projection area of this cell layer was delineated on the sections used for cell counting, and its projection area was measured on all analyzed sections using the above described stereology workstation and stereology software with the ×10/0.30 objective. This projection area, the corresponding average actual section thickness after histological preparation, and the distance between sections were used to calculate the total volume of the hippocampal pyramidal cell layer by means of Cavalieri's principle.[45] This method was also used to calculate the total volume of the hippocampus and its subfields.

An estimation of neuronal density in the anterior horn of the lumbar spinal cord of 12-month-old transgenic mice ($n = 3$) and wild-type mice ($n = 3$) was made with the optical disector method. For each animal, five coronal sections at 75-μm intervals were used. *Z*-stacks of sequential pictures of the anterior horn of the spinal cord were taken with an Axiocam camera and Axiovision software on a motorized light microscope (Zeiss Axiovert 200M) using a planapochromat ×63/1.40 oil objective. For each section, neurons were counted in two counting boxes (207 × 165 × 8 μm) randomly placed in the anterior horn of the spinal cord. All neurons whose nucleolus came into focus in the counting box disposed inside the *Z*-stack were counted in Image J software (National Institutes of Health, Bethesda, MD). The density of neurons was estimated from the numbers of counted neurons per volume of spinal gray matter estimated according to Cavalieri's principle.

Sciatic Nerves and Muscle Analysis

Sciatic nerve were dissected in transgenic and nontransgenic animals at 1, 3, and 12 months and fixed by immersion in 4% (w/v) glutaraldehyde in Millonig's buffer, pH 7.4, for 90 minutes. After washing in Millonig's buffer with 0.5% (w/v) glucose for 24 hours, the tissue samples were postfixed in 2% (w/v) OsO_4 for 30 minutes, dehydrated, and embedded in Epoxy resin LX112. Semithin cross sections (1 μm thickness) of the sciatic nerves were performed, stained with toluidine blue, photographed, and analyzed with the NIH Image J program: the total nerve area was measured using manual selection, and the total number of axons cross sections and their area were counted using the analyze particle function after image thresholding. Statistical analysis was performed using the Prism 4 software program (GraphPad Software). Blocks of tissue muscle from the quadriceps femoris were fixed in formalin, embedded in paraffin, and cut transversally to obtain cross sections of muscle fibers. Muscle tissue sections were stained with hematoxylin and eosin and the area of at least 50 muscle fibers/animal was manually measured with Image J.

Ultrastructural Analysis in Electron Microscopy

Control and transgenic animals were anesthetized with chloral hydrate and perfused intracardially with a solution of 2% (w/v) paraformaldehyde and 2% (v/v) glutaraldehyde in 0.1 mol/L phosphate buffer at pH 7.4. Tissue blocks of the spinal cord, sciatic nerves, hippocampus, and cerebral cortex were quickly dissected and further fixed by immersion in 4% (w/v) glutaraldehyde in 0.1 mol/L phosphate buffer at pH 7.4 for 90 minutes. After washing in Millonig's buffer with 0.5% (w/v) sucrose for 24 hours, the tissue blocks were postfixed in 2% (w/v) OsO_4 for 30 minutes, dehydrated, and embedded in Epon. Semithin sections were stained with toluidine blue. Ultrathin sections were counterstained with uranyl acetate and lead citrate and observed with a Zeiss EM 809 microscope at 80 kV. Measurements of the diameter of microtubules, neurofilaments, and abnormal filaments were performed on digitalized images.

Immunolabeling in Electron Microscopy

For immunolabeling, animals were perfused with a solution of 4% (w/v) paraformaldehyde and 0.5% (v/v) glutaraldehyde. Fifty-μm-thick tissue sections were cut on a vibratome, cryoprotected by incubation in 30% (w/v) sucrose, and frozen in isopentane cooled at −80°C. After thawing, the tissue sections were treated with 1% (w/v) sodium borohydride for 30 minutes and processed for immunolabeling with the ABC method, as reported.[8] Other tissue blocks were dehydrated, and embedded in LR White resin; the resin was polymerized at 50°C for 24 hours (Agar SL, UK). Ultrathin sections were used for postembedding immunolabeling with the immunogold method and the silver-enhancing method. In brief, ultrathin sections were incubated with 10% normal serum in Tris-buffered saline (0.1. mol/L Tris-HCl and 0.15 mol/L NaCl, pH 8.0) containing 1% normal serum, 0.1% Tween 20, 1% bovine serum albumin, 0.1% sodium azide for 10 minutes, followed by overnight incubation with the primary antibody diluted in the same buffer. After washing, the sections were incubated with gold-conjugated antibodies (BBInternational, Cardiff, UK), washed, and counterstained with lead citrate. For double labeling, sections were first immunolabeled with the primary antibody followed by a secondary antibody conjugated to biotin and streptavidin conjugated to 1-nm nanogold. The size of the nanogold particle was then enhanced for 2 minutes using a silver-enhancing solution (BBInternational). The silver

enhancement was followed by incubation with another primary antibody and a 10 nm-gold-conjugated secondary antibody.

Preparation and Examination of Sarkosyl-Insoluble Material

To investigate for the presence of PHF-like fibrillary material in transgenic mice, we used a protocol previously used to prepare fractions enriched in human PHF insoluble in Sarkosyl.[30] Brain tissue was homogenized in 10 mmol/L Tris/HCl, pH 7.4, 0.8 mol/L NaCl, 1 mmol/L ethylenediamine tetraacetic acid, and sucrose 10% (w/v) and centrifuged at 15,000 $\times$ *g* average for 20 minutes. The supernatant was mixed with Sarkosyl (1% w/v final) and centrifuged for 30 minutes at 100,000 $\times$ *g* average. The pellet containing the insoluble material was resuspended in 50 mmol/L Tris/HCl (pH 7.5). This material was adsorbed on Formvar-carbon-coated EM grids and negatively stained with potassium phosphotungstate and immunolabeled as reported[30] or analyzed by Western blotting.

Results

Tg30tau Mice Develop a Severe Motor Deficit with Neurogenic Muscle Atrophy and Axonopathy

The Tg30tau transgenic mice developed an ataxic gait and paresis of hindlimbs between 6 and 8 months of age. Dystonic postures were observed at more advanced stages. Tg30tau mice showed a clasping of the limbs rather than an escape posture as wild-type mice on tail elevation (Figure 1, A and B). Tg30tau mice exhibited a high degree of nervosity when tested by Rotarod before 8 months that impeded the significance of this motor testing before 8 months. The Rotarod testing confirmed, however, their progressive motor deficit after 8 months (Figure 1C). A significant difference between wild-type and Tg30tau transgenic mice was already observed at 8 months and dramatically worsened at 10 and 12 months. On dissection, severe muscle atrophy was observed in hindlimbs and extended to axial muscles and forelimbs in aged mice. Tissue samples of the quadriceps femoris showed groups of small angular muscle fibers in the Tgt30tau transgenic mice not present in wild-type mice (Figure 1, D and E). The mean cross-sectional area of muscle fibers in 11-month-old animals was significantly smaller in Tg30tau transgenic mice than in wild-type animals (Figure 1F). This severe motor phenotype precluded reliable demonstration of behavioral or cognitive disabilities in the Tg30tau line. This phenotype led to a reduced survival rate in Tg30 mice (Figure 1G), with a median survival of 12 months, whereas most wild-type littermates were still alive at this age.

Numerous myelin ovoids were detected on semithin sections of the sciatic nerve (Figure 2, A and B) in

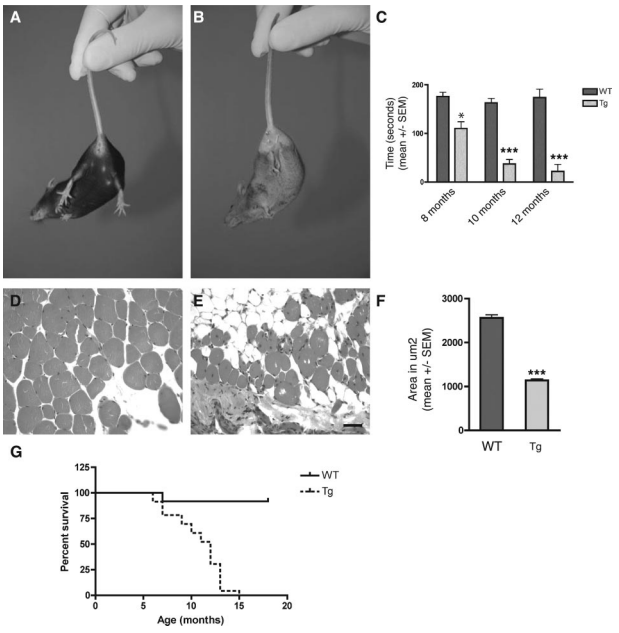

Figure 1. A and **B:** Tail test showing the abnormal limb-clasping reflex in a 12-month-old Tg30tau transgenic mouse (**B**) by comparison with an age-matched wild-type mouse (**A**). **C:** Rotarod testing of wild-type (n = 4 to 8 for each age) and Tg30tau (n = 7 to 13 for each age) transgenic mice at different ages. The time spent on the rotating rod by Tg30tau mice is already significantly shorter at 8 months and dramatically decreases at 10 and 12 months (two-way analysis of variance with Bonferroni post test). **D** and **E:** Tissue section showing the cross-sectional aspect of muscle fibers in the quadriceps femoris of 12-month-old wild-type (**D**) and Tg30tau (**E**) mice. **F:** There is a severe atrophy of muscle fibers in Tg30tau mice, as indicated by an important reduction in the mean cross-sectional area of muscle fibers in 11-month-old Tg30tau mice (n = 10) by comparison with wild-type mice (n = 4) (by Student's t-test). **G:** Kaplan-Meier survival curves showing the reduced survival of Tg30tau mice ($P < 0.0001$, by log-rank comparison). $^{*}P < 0.05$, $^{***}P < 0.001$. Scale bar = 60 μm.

12-month-old Tg30tau mice and ultrastructural examination showed an axonal degeneration with axonal loss and myelin destruction suggestive of Wallerian degeneration (Figure 2D). Abnormal axonal accumulations of multilamellar bodies and degraded mitochondria were also observed, already in 3-month-old Tg30 mice (Figure 2C). The number of axons in the sciatic nerve was similar in young wild-type and middle-aged Tg30tau animals but was significantly reduced in 12-month-old Tg30tau (Figure 2E). The axonal mean cross-sectional area increased with aging in wild-type animals but remained almost constant in Tg30tau mice and was significantly smaller at all ages in Tg30 tau mice (Figure 2F).

Tg30tau Mice Develop Brain and Hippocampal Atrophy in Absence of Overt Cell Loss

Brain weights were similar in wild-type and in Tg30tau transgenic mice at 3 and 6 months of age. However, a significant reduction in brain weight was observed at 12 months of age in Tg30tau transgenic mice (Figure 3A). The volume of the hippocampal formation was also significantly reduced in 12-month-old Tg30tau mice (Figure 3, B and D). Comparison of the volume of

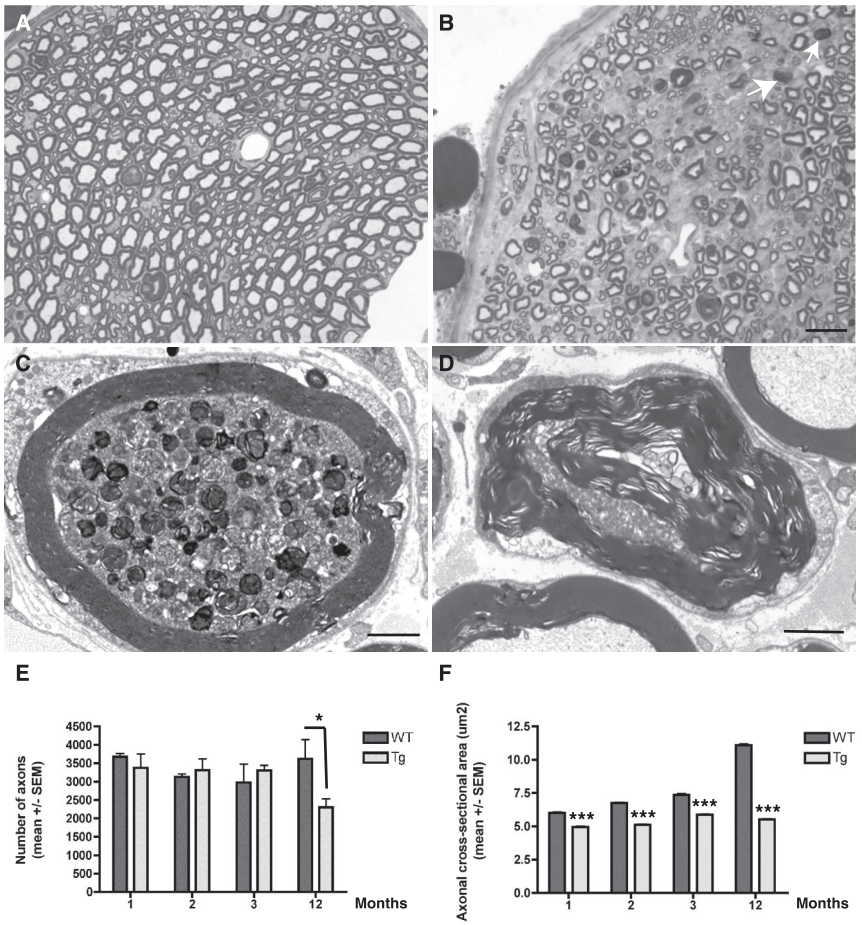

Figure 2. A and **B:** Semithin transverse sections of the sciatic nerve of 12-month-old wild-type (**A**) and Tg30tau (**B**) mice. There is a loss of myelinated axons in the Tg30tau mouse, and myelin ovoids are observed (**arrows** in **B**). **C** and **D:** Ultrastructural section of the sciatic nerve of Tg30tau mice. **C:** An axon shows accumulation of dense and lamellar bodies and degenerating mitochondria in a 3-month-old mouse. **D:** A degenerating axon is surrounded by a myelin sheath showing Wallerian degeneration in a 12-month-old mouse. **E**: The mean number of axonal profiles in transversal sections of the sciatic nerve is similar in young adult wild-type and Tg30tau mice but is significantly decreased in aged Tg30tau mice ($n = 3$ to 5 for wild-type and $n = 3$ to 6 for Tg30tau mice, at each age) (two-way analysis of variance with Bonferroni post test). **F:** The mean cross-sectional area of axons in the sciatic nerve is smaller in Tg30tau mice and increases with age in wild-type but not in Tg30tau mice (same animals as in **E**) (two-way analysis of variance with Bonferroni post test). $^{*}P < 0.05$, $^{***}P < 0.001$. Scale bars: 5 μm (**A** and **B**); 1.5 μm (**C** and **D**).

five different layers of the hippocampal formation (stratum radiatum, stratum oriens, pyramidal layer, molecular layer of the gyrus dentatus, and granule cell layer) showed a shrinkage of all layers, but only the volume of the stratum oriens ($P < 0.05$) and of the molecular layer of the gyrus dentatus ($P < 0.05$) were significantly decreased in Tg30 tau mice, suggesting that this volume reduction was more prominent in the dendritic field of granule cells and in the field of basal dendrites of pyramidal cells. The mean height of the primary dendritic shafts (MAP2-positive) was measured in the stratum oriens, in the stratum radiatum, and in the molecular layer of the gyrus dentatus and found to be significantly shorter in the stratum oriens of Tg30tau mice ($P < 0.05$, by Student's *t*-test) (Supplemental Figure 2, see *http://ajp.amjpathol.org*).

The number of neurons estimated with the optical fractionator method in the pyramidal cell layer of the hippocampus in 12-month-old animals was not found to be statistically different ($P = 0.805$, *t*-test) between wild-type and Tg30tau transgenic mice (Figure 3E). In the anterior horn of the lumbar spinal cord, the volumetric density of neurons was similar in 12-month-old wild-type and in Tg30 mice (Figure 3F) and was not associated to a change in the volume of spinal gray matter in the investigated level, indicating an absence of cell loss at this level. The TUNEL method detected a few rare positive nuclei in the cortex of 12-month-old transgenic mice but also in wild-type controls, and the anti-activated caspase was detected similarly in a few cells in Tg30tau mice and in wild-type mice.

Accumulation of Gallyas-Positive Inclusions in the Brain and in the Spinal Cord of Tg30tau Mice

The development of argyrophilic tau aggregates was studied with the Gallyas silver-staining method. Gallyas-positive neuronal inclusions in the cortex, the hippocampus, the brainstem, and the spinal cord was examined in 1-, 3-, 6-, and 11-month-old animals (Figure 4). Gallyas-positive neuronal inclusions were absent in 1-month-old Tg30tau mice. A few rare Gallyas-positive neuronal inclusions were detected in the cortex, in the pyramidal layer of the hippocampus and subicular areas (Figure 4A), and more in the gray matter of the spinal cord (Figure 4D) in 3-month-old mice. At 6 months, Gallyas-positive neuronal inclusions were systematically observed in the cortex and in the pyramidal layer of the hippocampus (Figure 4B) and were numerous in the spinal cord (Figure 4E). At 11 months, the numbers of Gallyas-positive neuronal inclusions dramatically increased in the brainstem and the spinal cord (where the majority of neuronal profiles were

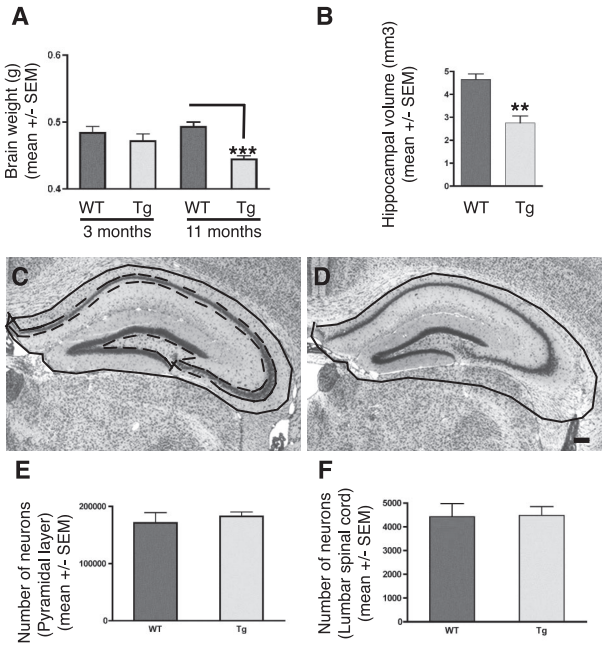

Figure 3. A: Brain weights of wild-type ($n = 4$ at 3 and 11 months) and Tg30tau ($n = 4$ at 3 months and $n = 11$ at 11 months) mice. The mean brain weight of Tg30tau mice is significantly decreased at 11 months of age but not at 3 months of age. $^{***}P < 0.001$ (one-way analysis of variance with Bonferroni post test). **B:** Hippocampal volumes of wild-type ($n = 3$) and Tg30tau ($n = 4$) mice at 12 months. The mean volume of the hippocampus is significantly decreased in 12-month-old Tg30tau mice. $^{**}P < 0.01$ (by Student's *t*-test). **C** and **D:** The neuroanatomical limits used for delineation of the hippocampal formation is shown as a solid black line in a wild-type mouse in **C** and is superposed on the hippocampal formation of a Tg30tau mouse in **D** to illustrate the decreased hippocampal area in the latter. The dashed line in **C** represents the limit of the area used to determine cell number in the pyramidal layer. **E** and **F:** Stereological analysis of cell number in the hippocampal pyramidal cell layer (**E**) and anterior horn of the lumbar spinal cord (**F**) of 12-month-old wild-type ($n = 3$) and Tg30tau ($n = 3$) mice. Total neuron numbers in the pyramidal layer of the hippocampus (**E**) and neuron numbers in the anterior horn of a limited segment of the lumbar spinal cord (**F**) of wild-type and Tg30tau mice were not different. Scale bar = 150 μm.

Gallyas-positive) (Figure 4F) and were frequent in the hippocampus (Figure 4C) and in the cortex. In aged animals, Gallyas-positive inclusions were also detected in deep cerebellar nuclei and in many subcortical nuclei. After Congo Red staining, a few of these fibrillary inclusions in the brain, but not in the spinal cord, showed a birefringence under crossed polarization filters and were thioflavin-positive.

Transgenic Human Tau Proteins Are Detected in Neurons in the Brain and Spinal Cord of Tg30tau Mice and Show Sequential Changes in Tau Phosphorylation, Conformation, and Solubility

The transgenic tau protein was expressed only in brain and spinal cord of Tg30tau mice and not in nonneuronal tissues (Figure 5A). The human tau protein, already detected at 18 days postnatally in transgenic mice, was expressed in cortical areas, in subcortical nuclei, in the brainstem, and in the spinal cord (Figure 5B). Numerous positive neurons with a somatodendritic labeling were detected in these areas, eg, in the hippocampus (Figure 5D) and in the spinal cord (Figure 5E). Many axonal tracts (eg, the corpus callosum, the mossy fibers, and the fimbria in the hippocampus) were also labeled. The transgenic tau protein was also detected in axons of the sciatic nerve (Figure 5F). Glial cells were not labeled.

We used a panel of tau antibodies to detect changes in tau phosphorylation and conformation in Tg30tau mice at different ages (18 days postnatally; 1, 3, 6, and 12 months old) (Table 1). Neurons with a positive somatodendritic labeling with AT180 and AT270 antibodies were detected as early as 18 days postnatally in the cortex and in the hippocampus and at 3 months in the spinal cord. MC1-, AP422-, and PHF-1-positive neurons were detected in spinal cord at 1 month and at 3 months in hippocampus. AT8-, pSer262-, and AT100-positive neurons were observed at 3 months both in the spinal cord and in the hippocampus and were concomitant with the appearance of Gallyas-positive neurons. We examined the development of somatodendritic accumulation of phosphotau with the AT8 antibody in 3-, 6-, and 11-month-old Tg30tau mice (Figure 6). The general pattern of evolution was similar as that observed with the Gallyas staining. In 3-month-old mice, rare AT8-positive neurons were detected in the cortex, in the pyramidal layer of the hippocampus and subicular areas (Figure 6A), and more in the gray matter of the spinal cord (Figure 6D). At 6 months, AT8-positive neurons were systematically observed in the cortex and in the pyramidal layer of the hippocampus (Figure 6B) and were numerous in the spinal cord (Figure 6E). At 11 months, the number of AT8-positive neurons dramatically increased in the spinal cord (Figure 6F) and these neurons were frequent in the hippocampus (Figure 6C) and in the cortex. Neurons with a positive somatodendritic labeling with all these tau antibodies were detected in 12-month-old Tg30tau mice (Figure 7, B–E) and also with anti-tau antibodies pThr212, pSer214, pThr403, and pSer409 (not shown) and were never observed in age-matched wild-type controls. Although most Gallyas-positive neurons were phosphotau-positive, Gallyas-negative neurons with a somatodendritic phosphotau labeling (eg, AT8) were also detected (Figure 13, C and E).

The antibodies to the N and C termini of human tau detected the early somatodendritic accumulation of human tau (Table 1) and also the initial neuronal fibrillary inclusions, suggesting that the whole human tau molecule is integrated into abnormal filaments. Neurons positively labeled with the anti-truncated tau (Asp421) were systematically observed only in 12-month-old Tg30tau mice (Figure 7G). The 4G10 and PT-66 phosphotyrosine antibodies strongly labeled fibrillary inclusions already in 3-month-old and older Tg30tau transgenic mice (Figure 7F). Double immunolabeling with the 4G10 and phosphotau antibodies showed a co-localization of the two immunoreactivities (not shown). Neurons positively labeled with the anti-ubiquitin antibodies were observed at 3 months and later (Figure 7H). The immunolabeling with the anti-GFAP antibody showed a slight increase in fibrillary astrocytes in the cortical areas and the hippocampus, more pronounced in the spinal cord. Microglial cells

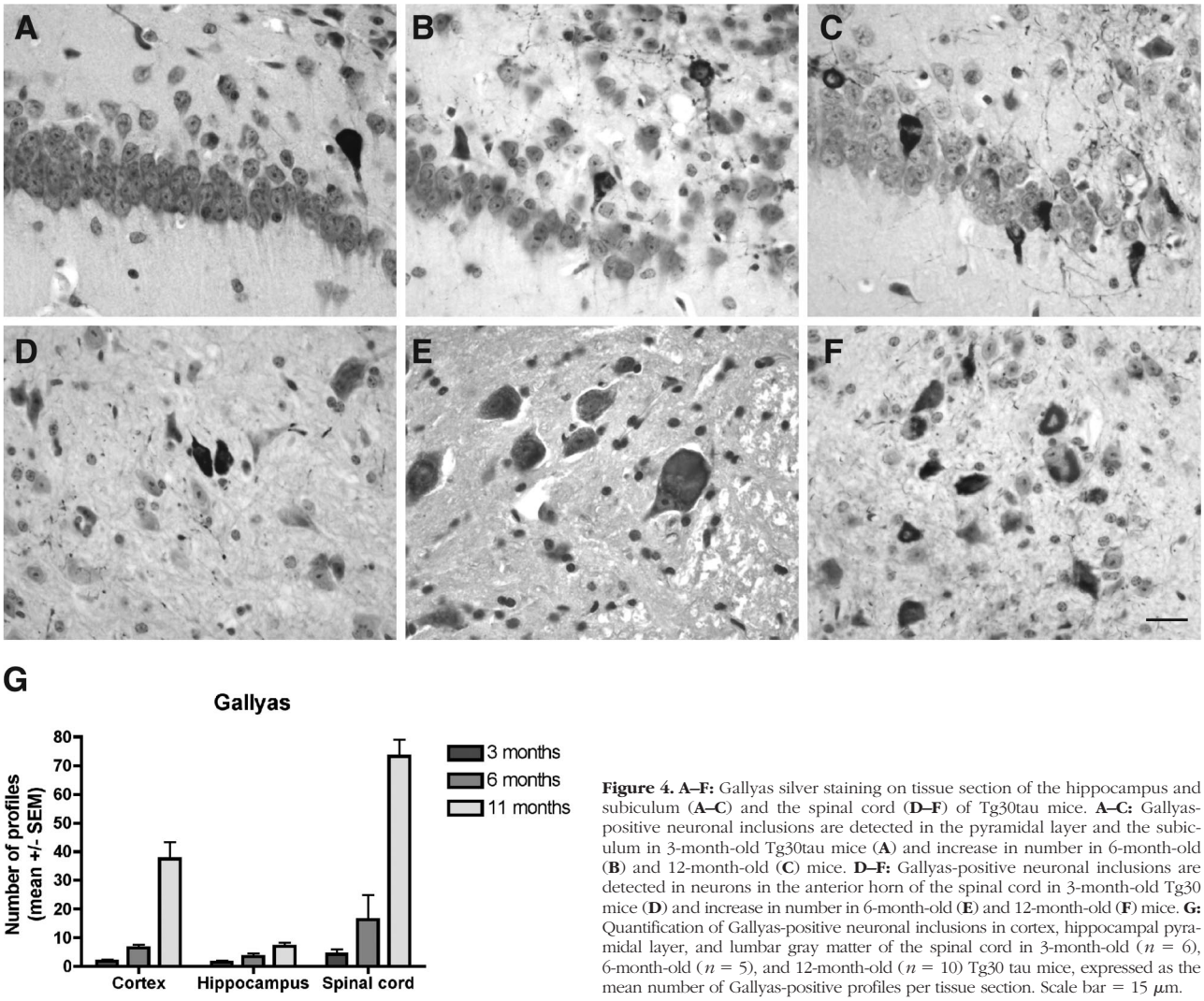

Figure 4. A–F: Gallyas silver staining on tissue section of the hippocampus and subiculum (**A–C**) and the spinal cord (**D–F**) of Tg30tau mice. **A–C:** Gallyas-positive neuronal inclusions are detected in the pyramidal layer and the subiculum in 3-month-old Tg30tau mice (**A**) and increase in number in 6-month-old (**B**) and 12-month-old (**C**) mice. **D–F:** Gallyas-positive neuronal inclusions are detected in neurons in the anterior horn of the spinal cord in 3-month-old Tg30 mice (**D**) and increase in number in 6-month-old (**E**) and 12-month-old (**F**) mice. **G:** Quantification of Gallyas-positive neuronal inclusions in cortex, hippocampal pyramidal layer, and lumbar gray matter of the spinal cord in 3-month-old (n = 6), 6-month-old (n = 5), and 12-month-old (n = 10) Tg30 tau mice, expressed as the mean number of Gallyas-positive profiles per tissue section. Scale bar = 15 μm.

detected with the RCA lectin were not more abundant in transgenic mice than in wild-type littermates.

The Western blot analysis of homogenates of brain and spinal cord of Tg30tau and wild-type mice with tau antibodies was performed at 3, 6, and 12 months of age (Figure 8). Tau species of 64- and 69-kd were detected with the human-specific tau antibody in brain and spinal cord at all ages in Tg30tau mice (Figure 8A), with the 69-kd species being more abundant in aged Tg30tau mice. These tau species were detected in Tg30tau mice already at 3 months with the phosphotau antibodies AD2 and AT100 (Figure 8, C and D) and at 6 months with the AT8 antibody (Figure 8B). The phosphotau antibodies AT180 and AT270 also detected these tau species at 3 months in Tg30tau mice (Supplemental Figure 3, see *http://ajp.amjpathol.org*).

Sarkosyl-insoluble material from the brain and the spinal cord was analyzed by Western blotting and examined by electron microscopy. In Tg30tau mice but not in wild-type controls, these preparations contained both 64- and 69-kd species immunoreactive with human-specific and phosphotau antibodies (Figure 9, A and B). In Tg30tau mice this material contained straight filaments or filaments with periodic constrictions. These filaments were immunolabeled with the human-specific TP20 tau antibody (Figure 9, C and D) and with the phosphotau AT8 antibody (Figure 9, E and F).

Spinal Cord but Not Hippocampal Fibrillary Inclusions Contain Neurofilaments

At the ultrastructural level, fibrillary large cytoplasmic inclusions were regularly detected in pyramidal neurons (Figure 10A) and in motorneurons in the spinal cord (Figure 10D). At higher magnification, the inclusions in the hippocampus were observed to be composed of bundles of parallel or swirling filaments that were often admixed with mitochondria (Figure 10B). Most of these filaments were straight or wavy (Figure 10C); measurement of their diameter on cross-sections gave values of 19.1 ± 0.2 nm (mean ± SEM, n = 50). For comparison, measurement of the diameter of adjacent microtubules in axons in the same transgenic animals gave values of 29.15 ± 0.3 nm (mean ± SEM, n = 36). Less often, filaments with regular constrictions were also encoun-

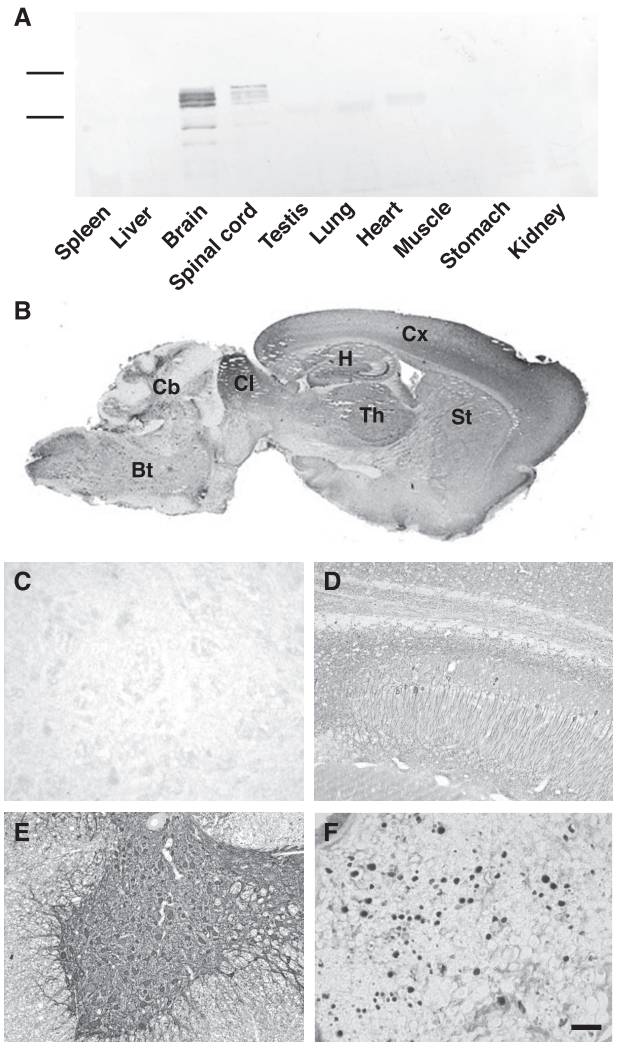

Figure 5. A: Western blotting analysis of the expression of the human tau transgenic protein in different organs of Tg30 mice with a human-specific antibody to tau. This expression is limited to brain and spinal cord. **B–F:** Immunocytochemical labeling with the human-specific antibody to tau. **B:** Low-magnification sagittal section of the brain of a 6-month-old Tg30tau mouse showing widespread expression of human tau in cortex (Cx), hippocampus (H), striatum (St), thalamus (Th), colliculus (CL), cerebellum (Cb), and brainstem (Bt). **C–F:** Higher magnification showing the strong expression of human tau in the pyramidal layer of the hippocampus (**D**), in the gray matter of the spinal cord (**E**), in the sciatic nerve (**F**), and its absence in the spinal cord of a wild-type mouse (**C**). Scale bar = 40 μm.

tered (Figure 10C); these PHF-like filaments had a larger diameter (35 nm) and regular constrictions (every 100 nm). Occasionally, continuity between the straight and PHF-like types of filaments was observed. The fibrillary inclusions in spinal cord motorneurons (Figure 10D) contained bundles of swirling thin 10-nm-wide filaments, sometimes admixed with the above-described 20-nm straight filaments (Figure 10F). These fibrillar inclusions tended to be relatively devoid of cytoplasmic organelles, eg, displacing them at the periphery of the cell body (Figure 10E).

In aged Tg30tau mice, most neurons with tau- and Gallyas-positive inclusions in the cortex and the hippocampus were not labeled by anti-NF antibodies (Figure 11, A and B). However, most neurons in the spinal cord and many neurons in brainstem nuclei contained inclusions immunolabeled with antibodies to tau and to phosphorylated and unphosphorylated NF-L, NF-M, and NF-H (Figure 11, C and D), already in 1-month-old Tg30tau mice (Table 1). Many neurons in the spinal cord had swollen cytoplasm and peripheral nuclei, consistent with chromatolytic features. Inclusions in spinal cord neurons were also Gallyas-positive at 3 months. The immunolabeling in electron microscopy indicated the presence of both tau and neurofilament immunoreactivities on separate filaments in the spinal cord inclusions (Figure 11E).

Axonal Dilatations and Spheroids Develop Early in the Cortex, Brainstem, and Spinal Cord of Tg30 Tau Mice

In addition to neurofilament-positive perikaryal inclusions, we detected frequent neurofilament-positive axonal dilatations and spheroids in the spinal cord (Figure 12C), in the brainstem (Figure 12D), in the cortex (Figure 12E), and more occasionally in the hippocampus. Spheroids were not present in 15-day-old Tg30tau mice but were detected in 1-month-old Tg30 tau mice and not in wild-type mice (Figure 12, A and B) before appearance of Gallyas-positive inclusions. These axonal spheroids were thus early lesions appearing before most tau phosphorylation changes, tau aggregation, and motor deficits (a timeline showing these events is presented in Supplemental Figure 1, see *http://ajp.amjpathol.org*).

Ultrastructural observations also identified spheroids that contained accumulations of membranous organelles (mitochondria, reticulum) and of microtubules and neurofilaments (Figure 12, F and G), indicative of impairment of axoplasmic transports. Abnormal multilamellar bodies and multivesicular bodies were frequently seen in these spheroids. Neuritic dilatations containing thick bundles of abnormal filaments often showed adjacent accumulations of normal and degraded organelles (Figure 12H), also suggestive of deficits of axoplasmic transports.

Protein Kinases GSK-3β and JNK Accumulate in Hippocampal Inclusions and ERK1 in Spinal Cord Inclusions

In view of the accumulation of phosphorylated tau in neurons, we investigated for potential changes in kinases/phosphatases distribution or expression in the brain of Tg30tau mice, using a panel of antibodies to selected kinases and phosphatases. In 6-month-old mice, we detected isolated neurons in the cortex and in the hippocampus with strong somatodendritic immunoreactivity for the active forms of GSK-3β (pY216) and of Jun kinase (Figure 13, A and B). Similar neurons were not detected with antibodies to kinases cdk5, p35, ERK1, casein kinase Id, or cdc2 and were not present in wild-type littermates. Double-immunolabeling with phospho-tau (AT8) and GSK-3β pY216 antibodies followed by Gallyas staining indicated that, among neurons showing

Table 1. Somatodendritic Immunoreactivity in Hippocampus and Spinal Cord of Tg30tau Mice

		Somatodendritic IR					
		1 month		3 months		12 months	
Antibody	Epitope	H	SC	H	SC	H	SC
B19*	Whole tau	+	+	+	+	+	+
TP20*	32-1	+	+	+	+	+	+
TP007*	1-6	+	+	+	+	+	+
TP70*	428-441	+	+	+	+	+	+
Asp421*	Tau cleaved at Asp421	−	−	−	−	+	+
AT270	Thr181 (P)	+	−	+	+	+	+
AT180	Thr231 (P)	+	−	+	+	+	+
PHF-1	Ser396/404 (P)	−	+	+	+	+	+
AP422	Ser422 (P)	−	+	+	+	+	+
MC1	7-9 and 312-342**	−	+	+	+	+	+
pSer262	Ser262 (P)	−	−	+	+	+	+
AT8	Ser202/Thr205 (P)	−	−	+	+	+	+
AT100	Thr212/Ser214***	−	−	+	+	+	+
4G10	Tyr (P)	−	−	+	+	+	+
Ubiquitin	ND	−	+	+	+	+	+
NA1214	NF-L	−	+	−	+	−	+
NA1216	NF-M	−	+	−	+	−	+
NA1211	NF-H (P)	−	+	−	+	−	+
Gallyas staining		−	−	+	+	+	+

The immunoreactivity was studied with phosphorylation-independent antibodies (*), antibodies requiring a phosphorylated epitope (P), a conformational epitope (**), or a conformational and phosphorylated epitope (***). The numbers refer to the position of amino acids in the longest human tau isoform. H, hippocampus; SC, spinal cord; +, present; −, absent. Gallyas silver staining was used to identify somatodendritic fibrillar aggregates.

an AT8 immunoreactivity at 6 months, the majority were also GSK-3β-positive (Figure 13, C and D) and Gallyas-positive (Figure 13E). Some AT8- and GSK-3β-positive neurons were however Gallyas-negative, suggesting that accumulation of phosphotau and GSK-3 might precede tau filament assembly. Neurons in spinal cord were also slightly GSK-3β-positive but most were strongly positive with the anti-ERK1 antibody (Figure 11F).

Discussion

A Transgenic Model for Tauopathies with Widespread Neurofibrillary Pathology and a Severe Motor Phenotype

In this study, we report the characterization of a new transgenic model expressing two pathogenic tau mutations identified in familial forms of FTD. P301S[23] and G272V[46] tau proteins have a reduced ability to promote microtubule assembly, and both mutations accelerate the formation of tau filaments *in vitro*.[47] The Tg30tau mice expressing this mutant tau developed NFTs both in the forebrain and in the spinal cord, as well as brain and hippocampal atrophy, axonopathy with neurogenic muscle atrophy and exhibited a reduced survival. These features were not observed in the previous transgenic line expressing the G272V mutation in a different tau isoform (2N4R) under a different promoter system (tetracycline-dependent transactivator system) and developing rather oligodendroglial fibrillary lesions.[13] Motor symptoms and NFTs developed in a transgenic line expressing the P301S mutation also in a different tau isoform (0N4R) but were observed in homozygous animals.[17] NFTs also developed in a recently described P301S transgenic tau line.[18] The motor and pathological phenotype of Tg30tau mice thus provides an adequate model for studying tauopathies in which brain and spinal cord NFT pathology is associated with a motorneuron disease such as FTD with motor signs[3] and the Guam-parkinsonism-amyotrophic lateral sclerosis-dementia complex.[48]

Different Neurofibrillary Lesions Develop in Forebrain and in Spinal Cord of Tg30tau Mice

Neurofibrillary lesions in brain and in spinal cord shared common features but also had distinct characteristics. Biochemical analysis showed the progressive accumulation of a phosphorylated 69-kd tau species in brain and spinal cord homogenates and in Sarkosyl-insoluble material. The sequence of early tau phosphorylation changes in the somatodendritic tau was different in forebrain and spinal cord: phosphorylated tau epitopes at Ser396/404 (PHF1), Ser422 (AP422), and a conformational tau epitope (MC1) appeared first in the spinal cord, whereas phosphorylated tau epitopes at Thr181 (AT270) and Thr231 (AT180) appeared first in forebrain, compatible with transgenic tau being initially a substrate for different protein kinases or combinations of protein kinases in these different neuronal populations. Phosphorylated tau epitopes at Ser202/Thr205 (AT8) and Ser262 (pSer262) and a phosphorylated/conformational tau epitope at Thr212/Ser214 (AT100) appeared later, in both the forebrain and the spinal cord. The first appearance of Gallyas-positive NFTs was concomitant of the latter phosphorylation events, suggesting that they either contribute to the aggregation process or indicate changes in kinase activities or in tau availability as a substrate for these kinases. Neurons at pretangle stage, phosphotau-positive and Gallyas-negative, were also present at

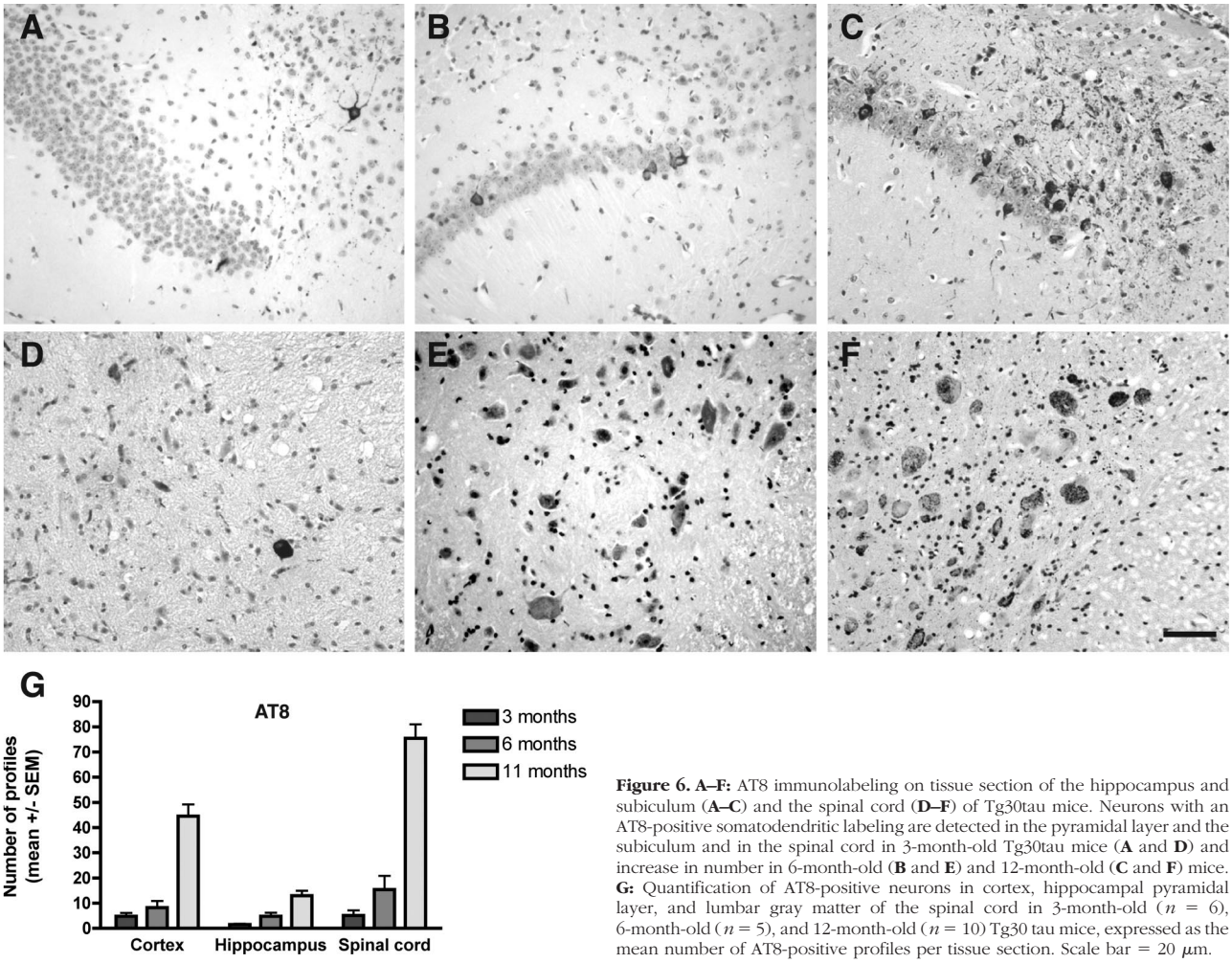

Figure 6. A–F: AT8 immunolabeling on tissue section of the hippocampus and subiculum (**A–C**) and the spinal cord (**D–F**) of Tg30tau mice. Neurons with an AT8-positive somatodendritic labeling are detected in the pyramidal layer and the subiculum and in the spinal cord in 3-month-old Tg30tau mice (**A** and **D**) and increase in number in 6-month-old (**B** and **E**) and 12-month-old (**C** and **F**) mice. **G:** Quantification of AT8-positive neurons in cortex, hippocampal pyramidal layer, and lumbar gray matter of the spinal cord in 3-month-old (n = 6), 6-month-old (n = 5), and 12-month-old (n = 10) Tg30 tau mice, expressed as the mean number of AT8-positive profiles per tissue section. Scale bar = 20 μm.

all ages. In the brain and the spinal cord, many neurons containing NFTs were labeled with antibodies to active GSK-3β and JNK suggesting that these protein kinases might be instrumental in generating at least some of the phosphotau epitopes identified in NFTs in Tg30tau mice. The association of GSK-3β with NFTs has been previously reported in AD[49,50] and in a P301L mutant tau transgenic line.[51] JNK phosphorylates tau *in vitro*[52] and was found associated to NFTs in a P301S mutant tau transgenic line.[17]

The NFTs were labeled with anti-tau antibodies specific for epitopes localized in the extreme N- and C-terminal domains of tau proteins, indicating that whole tau proteins were included in these inclusions. A labeling of NFTs with the antibody to truncated tau was observed only in more aged animals, suggesting that this proteolytic event is not a prerequisite for tau filament formation in Tg30tau line. This tau truncation has been reported to result from a caspase cleavage induced by extracellular Aβ and preceding apoptosis,[53] but we did not detect significant numbers of positive cells for active caspase nor apoptotic cells, and extracellular Aβ amyloid deposits were absent in Tg30tau mice.

In agreement with another study,[54] we detected phosphotyrosine immunoreactivity in NFTs, suggesting that the mutant tau protein was phosphorylated on tyrosine amino acid residues. Tyrosine phosphorylation of tau has been reported in AD brain,[55,56] and Aβ was found to induce tyrosine phosphorylation of tau,[57] but the present finding indicates that tyrosine phosphorylation of tau can also occur in the absence of Aβ.

Most NFTs in the forebrain were composed of both abundant straight or ribbon-like filaments and wider PHF-like filaments. Consistent with these observations, straight filaments have been reported in an FTD family with the P301S mutation,[23] and twisted filaments were observed in Pick's bodies of a family with hereditary Pick's disease with the G272V mutation.[58] In contrast, NFTs in spinal motorneurons contained a mixture of neurofilaments and abnormal tau-positive filaments and exhibited features of ballooned neurons. ERK1 immunoreactivity was also detected in NFTs in spinal cord but not in forebrain. ERK1 has been shown to phosphorylate neurofilament polypeptides[59] and might be responsible for the additional detection of phosphorylated neurofilament epitopes in these inclusions. Ballooned neurons have been found in human tauopathies and have been observed in a transgenic mouse line expressing mutant P301L human tau.[60] In the latter study, neurofilaments were also observed in these neurons by ultrastructural observation. Thus, expression of this double-mutant tau resulted in Tg30tau mice in contrasting differences in initial patterns of

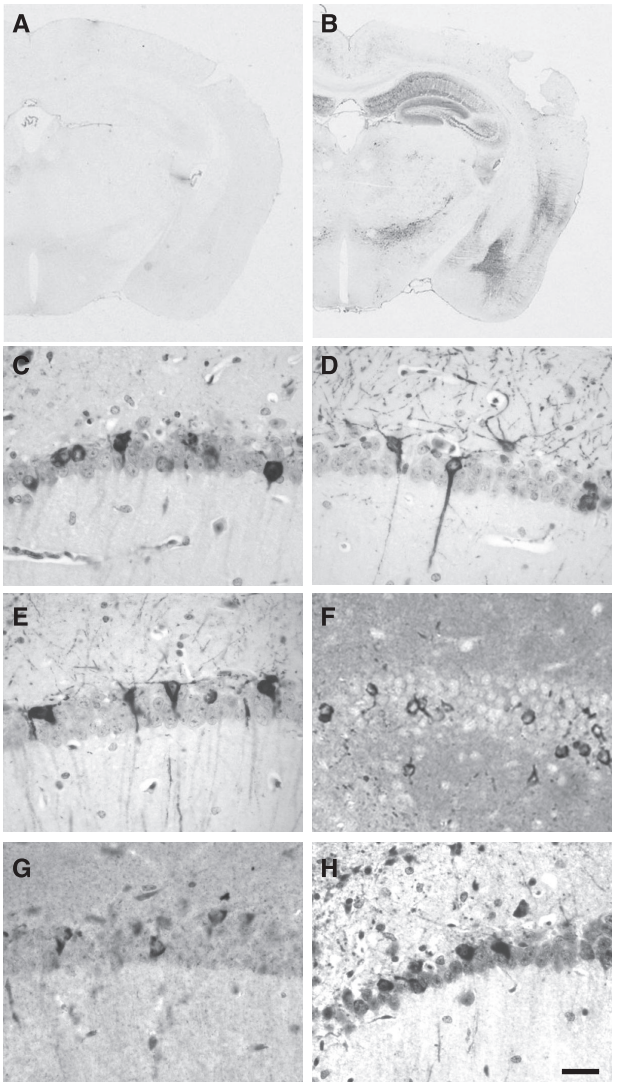

Figure 7. Immunocytochemical labeling with tau antibodies in 12-month-old Tg30tau mice. **A** and **B:** Low magnification showing the immunolabeling with the phospho-dependent tau antibody AT8 on a coronal section of a wild-type (**A**) and a Tg30tau (**B**) mouse. Note the strong AT8 labeling in the hippocampus and in the temporal cortex. **C–H:** Immunolabeling of NFTs on tissue section of the pyramidal layer of the hippocampus with the phospho-dependent tau antibodies AT180 (**C**) and PHF-1 (**D**), the conformation-dependent tau antibody MC1 (**E**), the phosphotyrosine 4G10 antibody (**F**), the anti-cleaved tau (Asp421) antibody (**G**), and the anti-ubiquitin antibody (**H**). Scale bar = 50 μm.

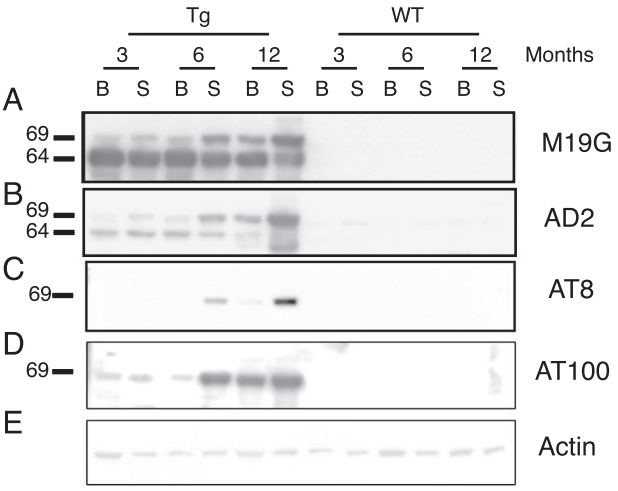

Figure 8. Western blot analysis of homogenates of brain (B) and spinal cord (S) of Tg30tau and wild-type mice at 3, 6, and 12 months of age. Equivalent protein yields (100 μg) were loaded in each lane. **A:** M19G human-specific tau antibody. The human transgenic tau protein is present at all ages inTg30 mice (and not in wild-type) as a 64-kd species but a slower migrating species of 69 kd is also detected at low level at 3 months and at higher level in 6- and 12-month-old Tg30tau mice. **B:** AD2 phosphotau antibody. The antibody detects both the 64- and the 69-kd species in Tg30tau mice, already at 3 months. **C:** AT8 phosphotau antibody. The antibody detects only the 69-kd species, a strong signal being first seen at 6 months in the spinal cord. **D:** AT100 conformation-dependent phosphotau antibody. The antibody detects only the 69-kd species, already at 3 months and in both the brain and the spinal cord. **E:** Actin antibody, used as a control for protein loading. The numbers on the left refers to the positions of PHF-tau proteins of 69 and 64 kd.

tau phosphorylation and later in recruitment or not of neurofilaments in tau-positive fibrillary inclusion in different neuronal populations.

Axonal Atrophy, Axonal Loss, and Spheroids as Evidence of Early Disturbances of Axoplasmic Transports

As reported previously,[61] we observed an age-dependent increase in the cross-sectional area of myelinated axons in the sciatic nerve of wild-type mice; the mean axonal cross-sectional area remained, however, relatively constant in Tg30tau mice, suggesting that mutant tau expression in Tg30tau mice interfered early with this axonal growth. The number of myelinated axons in the sciatic nerve was also reduced in aged Tg30tau mice, most probably explaining the neurogenic muscular atrophy observed in these animals. The axonal atrophy and loss were not associated with a significant change in neuronal density in the anterior horn of the spinal cord, suggesting that axons had degenerated in a number of these neurons but that their cell bodies were still present. This hypothesis is supported by the accumulation of phosphorylated neurofilaments in perikarya of spinal cord motor neurons in Tg30tau mice, an event known to be associated with a variety of axonal insults, including axonal transection[62,63] and several neurodegenerative diseases,[64] such as classic amyotrophic lateral sclerosis,[65] Guam amyotrophic lateral sclerosis/parkinsonism-dementia complex[48] and transgenic models.[66]

Axonal spheroids were numerous in Tg30tau mice and appeared even earlier than NFTs. An axonopathy with spheroids was observed in tau transgenic lines expressing wild-type tau,[9–11,67] but in the absence of NFTs. In agreement with our study, spheroids were also observed to occur early in a transgenic mouse strain expressing a wild-type 2N4R tau isoform and before NFTs when comparing the latter strain with a strain with an identical genetic background and expressing a mutant 2N4R tau isoform.[67] Spheroids differ, however, from the perikaryal inclusions in neurons of the spinal cord in Tg30tau mice because the latter are composed of a mixture of neurofilaments and abnormal tau-positive filaments. An ax-

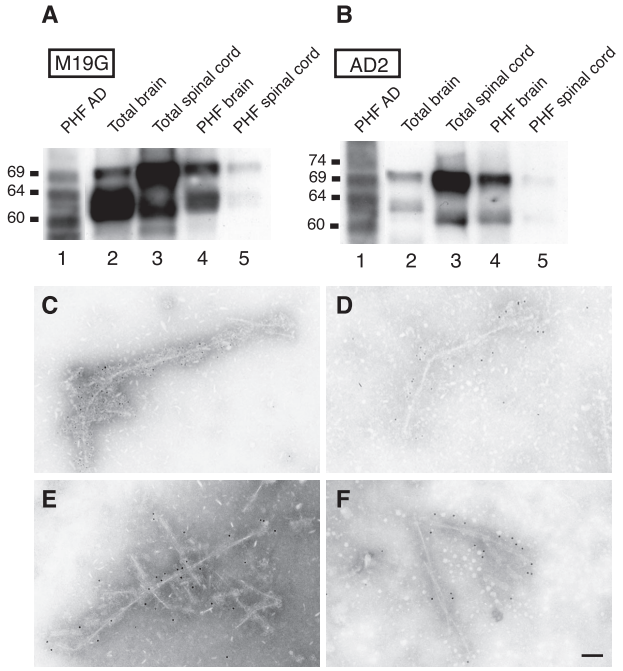

Figure 9. A and **B:** Western blot analysis with the human-specific antibody M19G (**A**) and the phospho-dependent tau antibody AD2 (**B**) of Sarkosyl-insoluble fractions from human AD brain (**lanes 1**), brain homogenates (**lanes 2**), spinal cord homogenates (**lanes 3**), and Sarkosyl-insoluble fractions from brain (**lanes 4**) and spinal cord (**lanes 5**) of 12-month-old Tg30tau mice. The 69- and a 64-kd species are detected in homogenates and Sarkosyl-insoluble fractions with both antibodies in Tg30tau mice, but the 69-kd species is more intensely immunoreactive than the 64-kd species with the AD2 antibody. Equivalent protein yields (100 μg) were loaded in **lanes 2** and **3**; similar volumes of resuspended Sarkosyl-insoluble material were loaded in **lanes 4** and **5**, but this material was obtained starting with 10 times more tissue weight for the brain by comparison with spinal cord. **C–F:** Immunogold labeling in electron microscopy of abnormal filaments present in the Sarkosyl fractions prepared from brain (**C** and **E**) and spinal cord (**D** and **F**) of Tg30tau mice. Filaments are labeled by the human-specific tau antibody TP20 (**C** and **D**) and the phospho-dependent tau antibody AT8 (**E** and **F**). Scale bar = 25 nm.

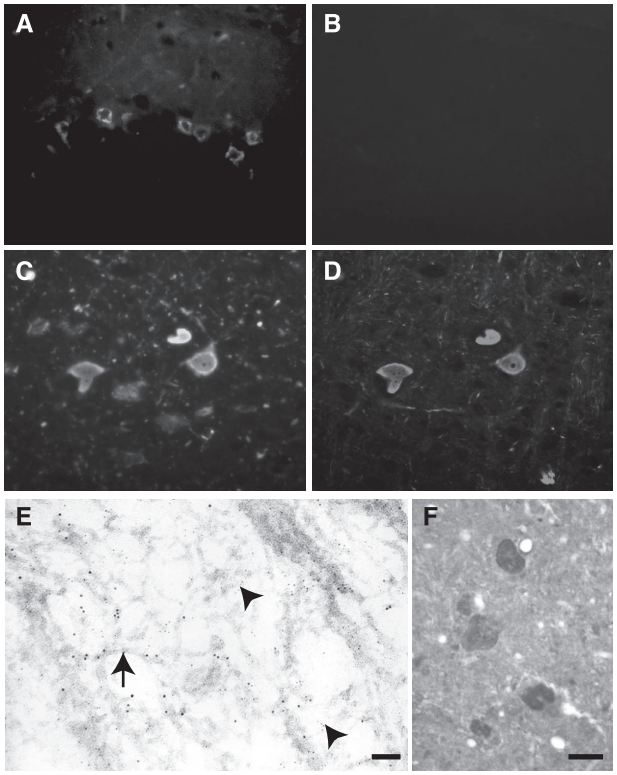

Figure 10. A–D: Double immunolabeling on tissue sections of the pyramidal layer of the hippocampus (**A** and **B**) and the anterior horn of the spinal cord (**C** and **D**) with the AT8 antibody (**A** and **C**) and the anti-neurofilament M antibody (**B** and **D**). The somatodendritic accumulation of phosphotau is associated to a neurofilament accumulation in motorneurons in the spinal cord but not in the pyramidal neurons in the hippocampus. **E:** Double immunogold labeling in electron microscopy (ultrathin section) of filaments present in a cytoplasmic inclusion in a spinal cord motor neuron with the AT8 (10-nm gold particles, **arrows**) and the anti-neurofilament M (5-nm gold particles, **arrowheads**) antibodies. **F:** Immunolabeling of cytoplasmic inclusions in spinal cord motorneurons with the anti-ERK1 antibody. Scale bars: 20 μm (**A–D**, **F**); 120 nm (**E**).

onopathy was also observed in some[14] but not all,[15,67] mutant tau transgenic lines developing NFTs in the spinal cord, but these NFTs were not neurofilament-positive, as in Tg30tau mice. Interestingly, cross-breeding of mice overexpressing wild-type tau with knockout mice devoid of one neurofilament polypeptide resulted in mice with reduced spheroid numbers and improved motor phenotype.[68] It seems thus possible that in Tg30tau mice the unique increased aggregating ability of the mutant tau (or any other toxic function) was further enhanced by direct or indirect interaction with neurofilaments and led to the development of a severe axonopathy and massive intraneuronal inclusions in spinal cord motor neurons. In addition to a functional defect of mutant tau (eg, on microtubule stability), it is possible that overexpression of tau per se plays also a role in development of the axonopathy. Segregation of cytoplasmic organelles by inclusions in spinal motor neurons, axonal spheroids, and accumulation of neurofilaments are all indicative of disturbances of axonal transport that would be the primary mechanism leading to early deficits in axonal growth and to later axonal degeneration in Tg30tau mice. Disturbance of axonal transports is thought to be a pathogenic mechanism in a variety of neurodegenerative diseases, including amyotrophic lateral sclerosis[65] and early stages of AD.[69] Additional early pathologies might also play a role in disease onset, eg, synapse loss as reported recently in a mutant tau model.[18]

Neurofibrillary Lesions and Hippocampal Atrophy Develop without Overt Neuronal Loss

Despite the presence of NFTs in the pyramidal layer, we did not observe a decrease in cell number in the same layer up to 12 months in Tg30tau mice. This result is consistent with a recent study in a reversible tau transgenic model indicating that existence of NFTs alone does not necessarily cause neuronal death in the forebrain.[16,22] However, Tg30tau mice developed age-dependent brain and hippocampal atrophy, and hippocampal atrophy was more marked in some dendritic fields, suggestive of shrinkage of dendritic arborization, in absence of marked cell loss Numerous neurons with somatodendritic phosphorylated tau, outnumbering the

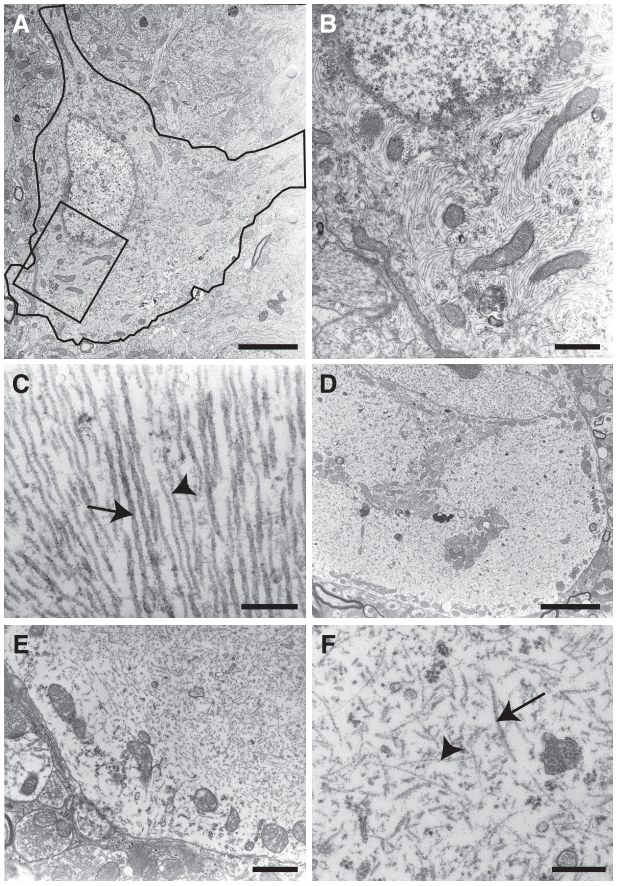

Figure 11. Ultrastructural aspects of fibrillary inclusions in the hippocampus (**A–C**) and in the spinal cord (**D–F**) of Tg30tau mice. **A:** A pyramidal neuron in the Ammon's horn contains numerous fibrillary inclusions in its cytoplasm. **B:** Higher magnification of the rectangular area delimited in **A**. Bundles of filaments are admixed with mitochondria. **C:** High magnification of a fibrillary inclusion composed of both straight filaments (**arrowhead**) and twisted filaments (**arrow**). **D:** A neuron in the anterior horn of the spinal cord contains a massive cytoplasmic inclusion. Organelles tend to be displaced in the center or at the periphery of the cytoplasm. **E:** Higher magnification showing the fibrillary aspect of the inclusion in a motor neuron and the peripheral position of mitochondria. **F:** High magnification of a motor neuron inclusion, showing the presence of both 20-nm straight filaments (**arrow**) and thin 10-nm filaments (**arrowhead**). Scale bars: 1 μm (**A** and **D**); 100 nm (**B**, **E**, and **F**); 300 nm (**C**).

number of NFTs, were observed in the hippocampi of Tg30 mice, and this high level of phosphorylated tau might be responsible for these neurodegenerative features. Aberrant tau phosphorylation, in the absence of NFT formation, is associated with tau-induced neurodegeneration in *Caenorhabditis elegans*,[70] *Drosophilia*,[71] and presenilin knockout mice.[72] Our data support the hypothesis that expression and phosphorylation of this mutant tau per se can exert deleterious effects on neuronal function without overt neuronal loss. However, this does not exclude the possibility that NFTs might have additional biological effects, eg, on axoplasmic flows. A similar conclusion can be drawn for NFTs in spinal cord: the axonal loss and atrophy in peripheral nerves demonstrates neuronal dysfunction, in the absence of overt changes in neuronal density despite impressive development of fibrillary inclusions. The Tg30tau mice thus provide an interesting model to investigate the relationship

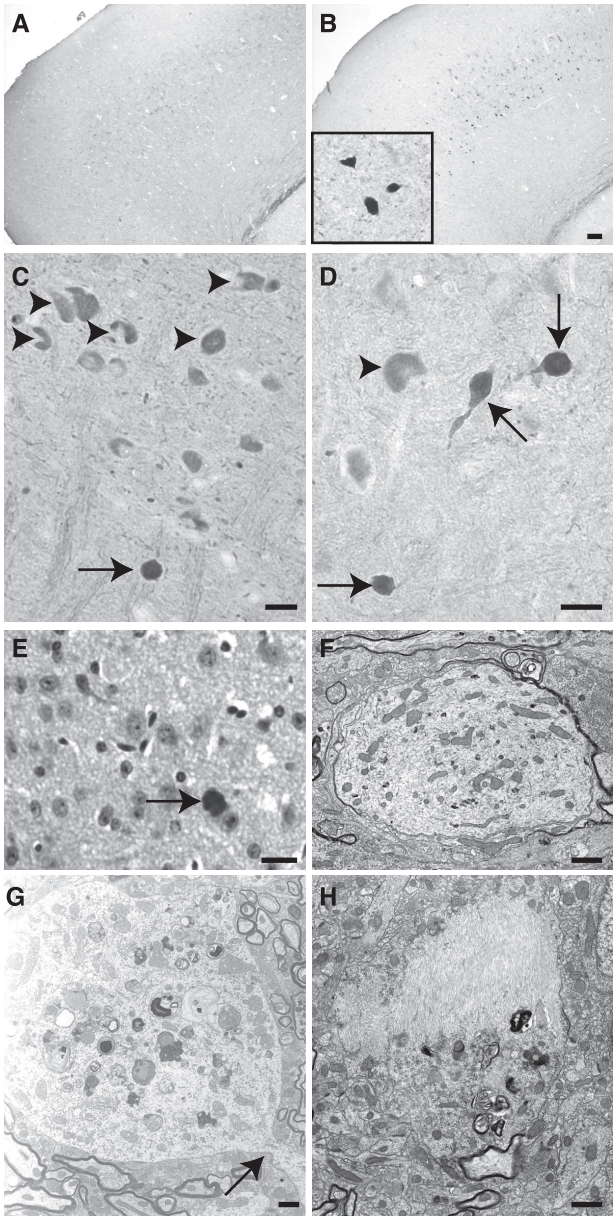

Figure 12. A–E: Anti-neurofilament labeling in 1-month-old (**A** and **B**) and 12-month-old (**C–E**) Tg30tau mice. **A** and **B:** Cortex. Neurofilament-positive spheroids are present in cortical layers of Tg30tau mice (**B** and **inset** in **B**) but not in wild-type mice (**A**). **C:** Spinal cord. Numerous neurons in the anterior horn show neurofilament-positive cytoplasmic inclusions (**arrowheads**). An axonal spheroid is also labeled (**arrow**). **D:** Brainstem. Three labeled spheroids continuous with small processes (**arrows**) are adjacent to a neuron with a positive cytoplasmic inclusion (**arrowhead**). **E:** Cortex. A labeled spheroid is identified (**arrow**). **F–H:** Ultrastructural aspects of axonal dilatations in Tg30tau mice. **F:** Hippocampal pyramidal layer. An axonal dilatation with an atrophic myelin sheath contains a disordered accumulation of mitochondria, membranous profiles, microtubules, and neurofilaments. **G:** Spinal cord. A marked neuritic dilatation contains accumulations of abnormal mitochondria, multilamellar and dense bodies, and Golgi stacks. The dilatation has a neck continuous with a process (**arrow**). **H:** Hippocampal pyramidal layer. A process contains a thick bundle of abnormal filaments adjacent to an abrupt accumulation of lamellar and dense bodies. Scale bars: 40 μm (**A** and **B**); 20 μm (**C** and **D**); 15 μm (**E**); 1.5 μm (**F** and **H**); 2.5 μm (**G**).

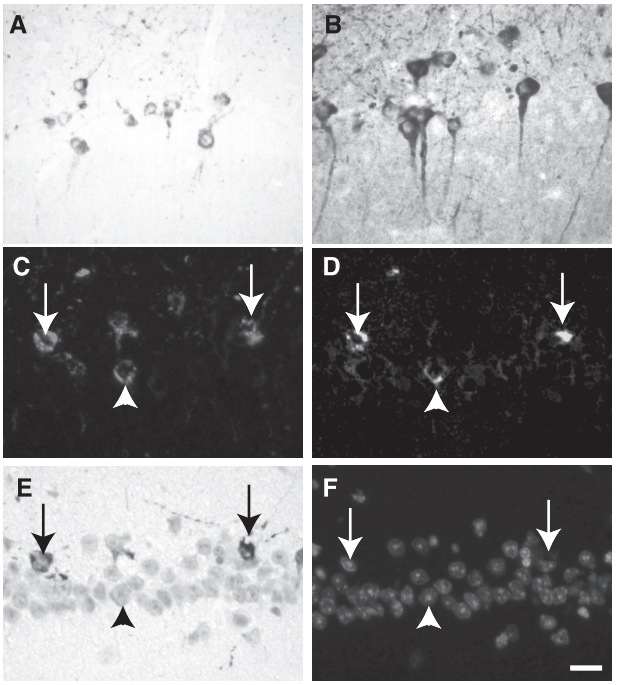

Figure 13. Immunocytochemical labeling on tissue section of the pyramidal layer of the hippocampus in 12-month-old Tg30tau mice. **A** and **B:** Immunolabeling of NFTs with the antibody to active Jun kinase (**A**) and to active GSK-3 (**B**). **C–F:** Quadruple labeling combining a double immunolabeling with the AT8 antibody (**C**) and the GSK-3 (pTyr216) antibody (**D**) and double staining with Gallyas (**E**) and 4,6-diamidino-2-phenylindole (**F**). Several neurons showing a somatodendritic phosphotau and GSK-3 immunoreactivity also contain Gallyas-positive inclusions (**arrows**), but some are not Gallyas-positive (**arrowheads**). Scale bar = 20 μm.

between tau fibrillary pathology, disturbances of axonal transport, cell death, and the selective vulnerability of neurons to form different types of fibrillary aggregates in neurodegenerative diseases.

Acknowledgments

We thank Drs. V. Baekelandt and E. Lauwers (Katholieke Universiteit Leuven, Belgium) for access and guidance to the stereology set-up facilities.

References

1. Lee VMY, Goedert M, Trojanowski JQ: Neurodegenerative tauopathies. Annu Rev Neurosci 2001, 24:1121–1159
2. Rodgers-Johnson P, Garruto RM, Yanagihara R, Chen KM, Gajdusek DC, Gibbs CJ Jr: Amyotrophic lateral sclerosis and parkinsonism-dementia on Guam: a 30-year evaluation of clinical and neuropathologic trends. Neurology 1986, 36:7–13
3. Lomen-Hoerth C, Anderson T, Miller B: The overlap of amyotrophic lateral sclerosis and frontotemporal dementia. Neurology 2002, 59:1077–1079
4. Kumar-Singh S, Van Broeckhoven C: Frontotemporal lobar degeneration: current concepts in the light of recent advances. Brain Pathol 2007, 17:104–113
5. Buée L, Bussière T, Buée-Scherrer V, Delacourte A, Hof PR: Tau protein isoforms, phosphorylation and role in neurodegenerative disorders. Brain Res Rev 2000, 33:95–130
6. Avila J, Lim F, Moreno F, Belmonte C, Cuello AC: Tau function and dysfunction in neurons—its role in neurodegenerative disorders. Mol Neurobiol 2002, 25:213–231
7. Götz J, Probst A, Spillantini MG, Schäfer T, Jakes R, Bürki K, Goedert M: Somatodendritic localization and hyperphosphorylation of tau protein in transgenic mice expressing the longest human brain tau isoform. EMBO J 1995, 14:1304–1313
8. Brion JP, Tremp G, Octave JN: Transgenic expression of the shortest human tau affects its compartmentalization and its phosphorylation as in the pretangle stage of Alzheimer disease. Am J Pathol 1999, 154:255–270
9. Ishihara T, Hong M, Zhang B, Nakagawa Y, Lee MK, Trojanowski JQ, Lee VMY: Age-dependent emergence and progression of a tauopathy in transgenic mice overexpressing the shortest human tau isoform. Neuron 1999, 24:751–762
10. Spittaels K, Van den Haute C, Van Dorpe J, Bruynseels K, Vandezande K, Laenen I, Geerts H, Mercken M, Sciot R, Van Lommel A, Loos R, Van Leuven F: Prominent axonopathy in the brain and spinal cord of transgenic mice overexpressing four-repeat human tau protein. Am J Pathol 1999, 155:2153–2165
11. Probst A, Götz J, Wiederhold KH, Tolnay M, Mistl C, Jaton AL, Hong M, Ishihara T, Lee VMY, Trojanowski JQ, Jakes R, Crowther RA, Spillantini MG, Bürki K, Goedert M: Axonopathy and amyotrophy in mice transgenic for human four-repeat tau protein. Acta Neuropathol (Berl) 2000, 99:469–481
12. Duff K, Knight H, Refolo LM, Sanders S, Yu X, Picciano M, Malester B, Hutton M, Adamson J, Goedert M, Burki K, Davies P: Characterization of pathology in transgenic mice over-expressing human genomic and cDNA tau transgenes. Neurobiol Dis 2000, 7:87–98
13. Götz J, Tolnay M, Barmettler R, Chen F, Probst A, Nitsch RM: Oligodendroglial tau filament formation in transgenic mice expressing G272V tau. Eur J Neurosci 2001, 13:2131–2140
14. Lewis J, McGowan E, Rockwood J, Melrose H, Nacharaju P, Van Slegtenhorst M, Gwinn-Hardy K, Murphy MP, Baker M, Yu X, Duff K, Hardy J, Corral A, Lin WL, Yen SH, Dickson DW, Davies P, Hutton M: Neurofibrillary tangles, amyotrophy and progressive motor disturbance in mice expressing mutant (P301L) tau protein. Nat Genet 2000, 25:402–405
15. Götz J, Chen F, Barmettler R, Nitsch RM: Tau filament formation in transgenic mice expressing P301L tau. J Biol Chem 2001, 276: 529–534
16. Santacruz K, Lewis J, Spires T, Paulson J, Kotilinek L, Ingelsson M, Guimaraes A, DeTure M, Ramsden M, McGowan E, Forster C, Yue M, Orne J, Janus C, Mariash A, Kuskowski M, Hyman B, Hutton M, Ashe KH: Tau suppression in a neurodegenerative mouse model improves memory function. Science 2005, 309:476–481
17. Allen B, Ingram E, Takao M, Smith MJ, Jakes R, Virdee K, Yoshida H, Holzer M, Craxton M, Emson PC, Atzori C, Migheli A, Crowther RA, Ghetti B, Spillantini MG, Goedert M: Abundant tau filaments and nonapoptotic neurodegeneration in transgenic mice expressing human P301S tau protein. J Neurosci 2002, 22:9340–9351
18. Yoshiyama Y, Higuchi M, Zhang B, Huang SM, Iwata N, Saido TC, Maeda J, Suhara T, Trojanowski JQ, Lee VM: Synapse loss and microglial activation precede tangles in a P301S tauopathy mouse model. Neuron 2007, 53:337–351
19. Tanemura K, Murayama M, Akagi T, Hashikawa T, Tominaga T, Ichikawa M, Yamaguchi H, Takashima A: Neurodegeneration with tau accumulation in a transgenic mouse expressing V337M human tau. J Neurosci 2002, 22:133–141
20. Tatebayashi Y, Miyasaka T, Chui DH, Akagi T, Mishima K, Iwasaki K, Fujiwara M, Tanemura K, Murayama M, Ishiguro K, Planel E, Sato S, Hashikawa T, Takashima A: Tau filament formation and associative memory deficit in aged mice expressing mutant (R406W) human tau. Proc Natl Acad Sci USA 2002, 99:13896–13901
21. Ikeda M, Shoji M, Kawarai T, Kawarabayashi T, Matsubara E, Murakami T, Sasaki A, Tomidokoro Y, Ikarashi Y, Kuribara H, Ishiguro K, Hasegawa M, Yen SH, Chishti MA, Harigaya Y, Abe K, Okamoto K, George-Hyslop PS, Westaway D: Accumulation of filamentous tau in the cerebral cortex of human tau R406W transgenic mice. Am J Pathol 2005, 166:521–531
22. Spires TL, Orne JD, SantaCruz K, Pitstick R, Carlson GA, Ashe KH, Hyman BT: Region-specific dissociation of neuronal loss and neurofibrillary pathology in a mouse model of tauopathy. Am J Pathol 2006, 168:1598–1607
23. Bugiani O, Murrell JR, Giaccone G, Hasegawa M, Ghigo G, Tabaton M, Morbin M, Primavera A, Carella F, Solaro C, Grisoli M, Savoiardo M, Spillantini MG, Tagliavini F, Goedert M, Ghetti B: Frontotemporal

dementia and corticobasal degeneration in a family with a P301S mutation in tau. J Neuropathol Exp Neurol 1999, 58:667–677
24. Hutton M, Lendon CL, Rizzu P, Baker M, Froelich S, Houlden H, Pickering-Brown S, Chakraverty S, Isaacs A, Grover A, Hackett J, Adamson J, Lincoln S, Dickson D, Davies P, Petersen RC, Stevens M, De Graaff E, Wauters E, Van Baren J, Hillebrand M, Joosse M, Kwon JM, Nowotny P: Association of missense and 5′-splice-site mutations in tau with the inherited dementia FTDP-17. Nature 1998, 393: 702–705
25. Heutink P, Stevens M, Rizzu P, Bakker E, Kros JM, Tibben A, Niermeijer MF, van Duijn CM, Oostra BA, van Swieten JC: Hereditary frontotemporal dementia is linked to chromosome 17q21–q22: a genetic and clinicopathological study of three Dutch families. Ann Neurol 1997, 41:150–159
26. Schindowski K, Bretteville A, Leroy K, Begard S, Brion JP, Hamdane M, Buee L: Alzheimer's disease-like tau neuropathology leads to memory deficits and loss of functional synapses in a novel mutated tau transgenic mouse without any motor deficits. Am J Pathol 2006, 169:599–616
27. Vidal M, Morris R, Grosveld F, Spanopoulou E: Tissue-specific control elements of the Thy-1 gene. EMBO J 1990, 9:833–840
28. Wirths O, Multhaup G, Czech C, Blanchard V, Tremp G, Pradier L, Beyreuther K, Bayer TA: Reelin in plaques of β-amyloid precursor protein and presenilin-1 double-transgenic mice. Neurosci Lett 2001, 316:145–148
29. Boutajangout A, Authelet M, Blanchard V, Touchet N, Tremp G, Pradier L, Brion JP: Cytoskeletal abnormalities in mice transgenic for human tau and familial Alzheimer's disease mutants of APP and presenilin-1. Neurobiol Dis 2004, 15:47–60
30. Brion JP, Hanger DP, Couck AM, Anderton BH: A68 proteins in Alzheimer's disease are composed of several tau isoforms in a phosphorylated state which affects their electrophoretic mobilities. Biochem J 1991, 279:831–836
31. Buée-Scherrer V, Condamines O, Mourton-Gilles C, Jakes R, Goedert M, Pau B, Delacourte A: AD2, a phosphorylation-dependent monoclonal antibody directed against tau proteins found in Alzheimer's disease. Mol Brain Res 1996, 39:79–88
32. Davis DR, Brion J-P, Couck A-M, Gallo J-M, Hanger DP, Ladhani K, Lewis C, Miller CCJ, Rupniak T, Smith C, Anderton BH: The phosphorylation state of the microtubule-associated protein tau as affected by glutamate, colchicine and b-amyloid in primary rat cortical neuronal cultures. Biochem J 1995, 309:941–949
33. Brion JP, Couck AM, Robertson J, Loviny TLF, Anderton BH: Neurofilament monoclonal antibodies RT97 and 8D8 recognize different modified epitopes in PHF-tau in Alzheimer's disease. J Neurochem 1993, 60:1372–1382
34. Goedert M, Jakes R, Vanmechelen E: Monoclonal antibody AT8 recognises tau protein phosphorylated at both serine 202 and threonine 205. Neurosci Lett 1995, 189:167–170
35. Goedert M, Jakes R, Crowther RA, Cohen P, Vanmechelen E, Vandermeeren M, Cras P: Epitope mapping of monoclonal antibodies to the paired helical filaments of Alzheimer's disease: identification of phosphorylation sites in tau protein. Biochem J 1994, 301:871–877
36. Hoffmann R, Lee VMY, Leight S, Varga I, Otvos L Jr: Unique Alzheimer's disease paired helical filament specific epitopes involve double phosphorylation at specific sites. Biochemistry 1997, 36:8114–8124
37. Hasegawa M, Jakes R, Crowther RA, Lee VMY, Ihara Y, Goedert M: Characterization of mAb AP422, a novel phosphorylation-dependent monoclonal antibody against tau protein. FEBS Lett 1996, 384:25–30
38. Otvos L Jr, Feiner L, Lang E, Szendrei GI, Goedert M, Lee VM-Y: Monoclonal antibody PHF-1 recognizes tau protein phosphorylated at serine residues 396 and 404. J Neurosci Res 1994, 39:669–673
39. Jicha GA, Bowser R, Kazam IG, Davies P: Alz-50 and MC-1, a new monoclonal antibody raised to paired helical filaments, recognize conformational epitopes on recombinant tau. J Neurosci Res 1997, 48:128–132
40. Brion JP, Couck AM, Bruce M, Anderton BH, Flament-Durand J: Synaptophysin and chromogranin A immunoreactivities in senile plaques of Alzheimer's disease. Brain Res 1991, 539:143–150
41. Boutajangout A, Leroy K, Touchet N, Authelet M, Blanchard V, Tremp G, Pradier L, Brion JP: Increased tau phosphorylation but absence of formation of neurofibrillary tangles in mice double transgenic for human tau and Alzheimer mutant (M146L) presenilin-1. Neurosci Lett 2002, 318:29–33
42. West MJ, Slomianka L, Gundersen HJ: Unbiased stereological estimation of the total number of neurons in the subdivisions of the rat hippocampus using the optical fractionator. Anat Rec 1991, 231: 482–497
43. Williams RW, Rakic P: Three-dimensional counting: an accurate and direct method to estimate numbers of cells in sectioned material. J Comp Neurol 1988, 278:344–352
44. Schmitz C, Hof PR: Recommendations for straightforward and rigorous methods of counting neurons based on a computer simulation approach. J Chem Neuroanat 2000, 20:93–114
45. Cavalieri B: Geometria Degli Indivisibili [from Cavalieri (1635) Geometria Indivisibilibus Continuorum. Bononiae: Typis Clementis Ferronij]. Italian. Torino, Unione Tipografico-Editrice Torinese, 1966
46. Hasegawa M, Smith MJ, Goedert M: Tau proteins with FTDP-17 mutations have a reduced ability to promote microtubule assembly. FEBS Lett 1998, 437:207–210
47. Goedert M, Jakes R, Crowther RA: Effects of frontotemporal dementia FTDP-17 mutations on heparin-induced assembly of tau filaments. FEBS Lett 1999, 450:306–311
48. Shankar SK, Yanagihara R, Garruto RM, Grundke-Iqbal I, Kosik KS, Gajduzek DC: Immunocytochemical characterization of neurofibrillary tangles in amyotrophic lateral sclerosis and Parkinsonism-dementia of Guam. Ann Neurol 1989, 25:146–151
49. Pei JJ, Braak E, Braak H, Grundke-Iqbal I, Iqbal K, Winblad B, Cowburn RF: Distribution of active glycogen synthase kinase 3β (GSK-3β) in brains staged for Alzheimer disease neurofibrillary changes. J Neuropathol Exp Neurol 1999, 58:1010–1019
50. Leroy K, Yilmaz Z, Brion JP: Increased level of active GSK-3β in Alzheimer's disease and accumulation in argyrophilic grains and in neurons at different stages of neurofibrillary degeneration. Neuropathol Appl Neurobiol 2007, 33:43–55
51. Ishizawa T, Sahara N, Ishiguro K, Kersh J, McGowan E, Lewis J, Hutton M, Dickson DW, Yen SH: Co-localization of glycogen synthase kinase-3 with neurofibrillary tangles and granulovacuolar degeneration in transgenic mice. Am J Pathol 2003, 163:1057–1067
52. Reynolds CH, Betts JC, Blackstock WP, Nebreda AR, Anderton BH: Phosphorylation sites on tau identified by nanoelectrospray mass spectrometry: differences in vitro between the mitogen-activated protein kinases ERK2, c-Jun N-terminal kinase and P38, and glycogen synthase kinase-3β. J Neurochem 2000, 74:1587–1595
53. Gamblin TC, Chen F, Zambrano A, Abraha A, Lagalwar S, Guillozet AL, Lu ML, Fu YF, Garcia-Sierra F, LaPointe N, Miller R, Berry RW, Bincler LI, Cryns VL: Caspase cleavage of tau: linking amyloid and neurofibrillary tangles in Alzheimer's disease. Proc Natl Acad Sci USA 2003, 100:10032–10037
54. Vega IE, Cui L, Propst JA, Hutton ML, Lee G, Yen SH: Increase in tau tyrosine phosphorylation correlates with the formation of tau aggregates. Mol Brain Res 2005, 138:135–144
55. Lee G, Thangavel R, Sharma VM, Litersky JM, Bhaskar K, Fang SM, Do LH, Andreadis A, Van Hoesen G, Ksiezak-Reding H: Phosphorylation of tau by fyn: implications for Alzheimer's disease. J Neurosci 2004, 24:2304–2312
56. Derkinderen P, Scales TME, Hanger DP, Leung KY, Byers HL, Ward MA, Lenz C, Price C, Bird IN, Perera T, Kellie S, Williamson R, Noble W, Van Etten RA, Leroy K, Brion JP, Reynolds CH, Anderton BH: Tyrosine 394 is phosphorylated in Alzheimer's paired helical filament tau and in fetal tau with c-Abl as the candidate tyrosine kinase. J Neurosci 2005, 25:6584–6593
57. Williamson R, Scales T, Clark BR, Gibb G, Reynolds CH, Kellie S, Bird IN, Varndell IM, Sheppard PW, Everall I, Anderton BH: Rapid tyrosine phosphorylation of neuronal proteins including tau and focal adhesion kinase in response to amyloid-β peptide exposure: involvement of src family protein kinases. J Neurosci 2002, 22:10–20
58. Bronner IF, ter Meulen BC, Azmani A, Severijnen LA, Willemsen R, Kamphorst W, Ravid R, Heutink P, van Swieten JC: Hereditary Pick's disease with the G272V tau mutation shows predominant three-repeat tau pathology. Brain 2005, 128:2645–2653
59. Veeranna, Amin ND, Ahn NG, Jaffe H, Winters CA, Grant P, Pant HC: Mitogen-activated protein kinases (Erk1,2) phosphorylate Lys-Ser-Pro (KSP) repeats in neurofilament proteins NF-H and NF-M. J Neurosci 1998, 18:4008–4021
60. Lin WL, Lewis J, Yen SH, Hutton M, Dickson DW: Ultrastructural neuronal pathology in transgenic mice expressing mutant (P301L) human tau. J Neurocytol 2003, 32:1091–1105

61. Samorajski T: Age differences in the morphology of posterior tibial nerves of mice. J Comp Neurol 1974, 157:439–445
62. Goldstein ME, Cooper HS, Bruce J, Carden MJ, Lee VM, Schlaepfer WW: Phosphorylation of neurofilament proteins and chromatolysis following transection of rat sciatic nerve. J Neurosci 1987, 7:1586–1594
63. Rosenfeld J, Dorman ME, Griffin JW, Gold BG, Sternberger LA, Sternberger NH, Price DL: Distribution of neurofilament antigens after axonal injury. J Neuropathol Exp Neurol 1987, 46:269–282
64. Dickson DW, Yen SH, Suzuki KI, Davies P, Garcia JH, Hirano A: Ballooned neurons in select neurodegenerative diseases contain phosphorylated neurofilament epitopes. Acta Neuropathol (Berl) 1986, 71:216–223
65. Munoz DG, Greene C, Perl DP, Selkoe DJ: Accumulation of phosphorylated neurofilaments in anterior horn motoneurons of amyotrophic lateral sclerosis patients. J Neuropathol Exp Neurol 1988, 47:9–18
66. Götz J, Deters N, Doldissen A, Bokhari L, Ke YZ, Wiesner A, Schonrock N, Ittner LM: A decade of tau transgenic animal models and beyond. Brain Pathol 2007, 17:91–103
67. Terwel D, Lasrado R, Snauwaert J, Vandeweert E, Van Haesendonck C, Borghgraef P, Van Leuven F: Changed conformation of mutant tau-P301L underlies the moribund tauopathy, absent in progressive, nonlethal axonopathy of tau-4R/2N transgenic mice. J Biol Chem 2005, 280:3963–3973
68. Ishihara T, Higuchi M, Zhang B, Yoshiyama Y, Hong M, Trojanowski JQ, Lee VMY: Attenuated neurodegenerative disease phenotype in tau transgenic mouse lacking neurofilaments. J Neurosci 2001, 21:6026–6035
69. Stokin GB, Lillo C, Falzone TL, Brusch RG, Rockenstein E, Mount SL, Raman R, Davies P, Masliah E, Williams DS, Goldstein LSB: Axonopathy and transport deficits early in the pathogenesis of Alzheimer's disease. Science 2005, 307:1282–1288
70. Kraemer BC, Zhang B, Leverenz JB, Thomas JH, Trojanowski JQ, Schellenberg GD: Neurodegeneration and defective neurotransmission in a Caenorhabditis elegans model of tauopathy. Proc Natl Acad Sci USA 2003, 100:9980–9985
71. Wittmann CW, Wszolek MF, Shulman JM, Salvaterra PM, Lewis J, Hutton M, Feany MB: Tauopathy in Drosophila: neurodegeneration without neurofibrillary tangles. Science 2001, 293:711–714
72. Saura CA, Choi SY, Beglopoulos V, Malkani S, Zhang DW, Rao BSS, Chattarji S, Kelleher Iii RJ, Kandel ER, Duff K, Kirkwood A, Shen J: Loss of presenilin function causes impairments of memory and synaptic plasticity followed by age-dependent neurodegeneration. Neuron 2004, 42:23–36